Non-Invasive Systems for Out-of-Clinic Monitoring of Biomechanical Measures

A Dissertation
Presented to
The Academic Faculty

by

Jordan L. Conant

In Partial Fulfillment
of the Requirements for the Degree
Master of Science in the
School of Electrical and Computer Engineering]

Georgia Institute of Technology
December 2016

Non-Invasive Systems for Out-of-Clinic Monitoring of Biomechanical Measures

Approved by:

Dr. Omer T. Inan, Advisor
School of Electrical and Computer Engineering
Georgia Institute of Technology

Dr. Hua Wang
School of Electrical and Computer Engineering
Georgia Institute of Technology

Dr. Mindy L. Millard-Stafford
School of Applied Physiology
Georgia Institute of Technology

Date Approved: [Month dd, yyyy]

ACKNOWLEDGEMENTS

I would like to thank my family, especially my parents, for their continued support for me throughout every phase of my life. In addition I would like to thank my research advisor Dr. Omer T. Inan for allowing me to have the opportunity to research in his lab; I will be forever grateful for the knowledge and experience I have gained during this research. To my reading committee, Dr. Hua Wang and Dr. Mindy Millard-Stafford – I appreciate your willingness to serve and advise me during this exciting phase of my life. Finally, I would like to thank all of my lab-mates especially Andrew Carek, Caitlin Teague, Nick Bolus, and Oludotun Ode for making my time in lab such a great experience.

TABLE OF CONTENTS

LIST OF TABLES

LIST OF FIGURES

LIST OF SYMBOLS AND ABBREVIATIONS

AFE	Analog front-end
AO	Aortic opening
BCG	Ballistocardiogram
BP	Blood pressure
BPV	Blood pressure variability
CPU	Central processing unit
CVD	Cardiovascular disease
DBP	Diastolic blood pressure
EBI	Electrical bio-impedance
ECG	Electrocardiogram
EP	Epidermal Pulse
HPF	High-pass filter
ICG	Impedance cardiogram
IMU	Inertial measurement unit
LED	Light emitting diode
LPF	Low-pass filter
MAP	Mean arterial pressure
MRI	Magnetic resonance imaging
OA	Osteoarthritis
PAT	Pulse arrival time
PD	Photodiode
PEP	Pre-ejection period

PPG	Photoplethysmogram
RF	Radio frequency
RFI	Radio frequency interference
SBP	Systolic blood pressure
SCG	Seismocardiogram
SpO2	Oxygen saturation of pulsatile blood
TIA	Transimpedance amplifier
UI	User interface
VI	Virtual instrument

SUMMARY

The ability to more continuously record out-of-clinic data is a critical component in the progress from the current hospital-centered healthcare system, which will continue to be stressed by the growing aging population, to one that is preventative and pervasive. In order to achieve this healthcare model, the development of robust acquisition systems which can be used in daily life for recording biomechanical measures is crucial. Chronic diseases such as osteoarthritis and cardiovascular disease affect a large portion of aging adults and pose an immense financial burden on healthcare.

This research investigates novel technologies for sensing clinically-relevant parameters for both of these prevalent disease groups, with a shared focus on wearable or unobtrusive biomechanical measurements. Specifically, knee joint acoustics and the vibrations of the body in response to the heartbeat are studied. Both sets of measurements required the development of low-noise, analog front-end circuits, together with robust packaging tailored to facilitate high quality recordings in unsupervised settings. These systems are expected to provide high-quality data capture, while also maximizing user adherence and convenience.

CHAPTER 1. INTRODUCTION

Mortality rates due to communicable diseases continue to decline across the globe, confirming modern healthcare's ability to identify and treat infectious diseases. This feat, in addition to other factors, has led to the population of adults over the age of 65 being the most rapidly growing demographic worldwide [1]. Unfortunately, these aging adults are highly susceptible to developing chronic diseases such as cardiovascular disease (CVD), diabetes, and arthritis. In fact, a 2008 study of adults in the United States over the age of 65 showed that 92.2% reported suffering from one or more chronic diseases and 17.4% reported suffering from four or more chronic diseases representing an increase in both cases from 86.9% and 11.7%, respectively, in 1998 [2].

The subsequent effects of increased chronic disease rates and the resulting burdens on healthcare systems and economies across the globe have become evident – in 2002 healthcare related costs of heart disease alone reached over $351 billion in the United States [3]. The working age population is dramatically affected by chronic disease as well. The United States lost an estimated $3.3 trillion between 1994 and 2005 because of disability-related costs for medical care and lost productivity [4]. Of the 47.5 million Americans on disability, 40% can be attributed to arthritis, spinal problems, and heart related diseases [4]. Part of this immense financial burden can be attributed to the current hospital-centered healthcare system's inefficiency in managing chronic diseases and to expensive interventions used for treatments that often do not solve the underlying cause of the physiological problem.

In contrast, if at-risk populations were continuously monitored, they could potentially be treated with preventative measures such as medication, physical therapy, and behavior modification upon risk identification in an attempt to prevent, or at least slow, chronic disease progression. This kind of health management system would be personalized, data driven, and more cost effective than traditional hospital-centered care. The acknowledgement of this reality has begun to change the approach of some healthcare research toward a "p-health" system in which healthcare will become "preventive, predictive, preemptive, personalized, pervasive, participatory, patient-centered, and precise" [5]. To widen participation, mainstream devices such as smartphones and watches have already begun to incorporate systems to encourage healthier lifestyle choices by measuring and conveying information to the user pertaining to heart rate, activity level, etc. [6]. For more complete care, however, more specialized solutions for out-of-clinic monitoring of at-risk individuals must be pursued. This document will focus specifically on research for medical systems based on biomechanical sensing used to monitor joint and cardiovascular health with the intent to give healthcare providers the ability to obtain more continuous out-of-clinic patient data, provide quantitative feedback for recovery characterization, or help monitor and identify early risk factors in at-risk populations.

1.1 Osteoarthritis

Osteoarthritis (OA) is the most common chronic joint disease, typically manifesting in the hips, knees, and hands of older adults. Nearly 50% of all adults over the age of 65 have some form of arthritis, and by 2040 it is estimated that nearly 80 million American adults will be diagnosed with the disease – placing an immense burden on the current healthcare system [7]. Currently pain is the first symptom which motivates an individual

to see their doctor to be assessed for arthritis; however, since articular cartilage is not innervated, pain does not typically manifest itself early enough for pharmacological treatment to significantly impact the prognosis of the affected individual [8]. While additional clinically relevant symptoms of OA differ depending on the joint affected, crepitus, joint space narrowing, and stiffness are common to all affected joints such as the knee, hip, and hand. Treatment of OA is usually a combination of physical therapy, non-steroidal anti-inflammatory drugs or weak opioids, and exercise; severe cases of OA may require surgical procedures. However, the weight loss which results unloading the arthritic joint has shown to be the most effective treatment for the OA in the hip and knee [9].

The most commonly employed method for OA assessment is X-ray radiology due to accessibility, relatively low cost, and ability to view joints in weight-bearing conditions [8, 10]. However, continuous monitoring of OA with this method is not sufficiently dynamic as it can take more than a year for significant changes in joint space to become evident [11-14]. In addition, there are currently no known biomarkers which can aid in the early diagnosis of or in determining the prognosis for OA. If such a biomarker was identified, it may provide a more continuous and affordable method for early risk-factor identification and recovery monitoring for pre-emptive treatment and quantitative classification of recovery for OA.

The ability to study knee joint acoustics as a biomarker for the severity of and recovery from musculoskeletal disease and injury has been shown to provide significant potential as a low-cost alternative in proof-of-concept studies [10, 15]. The first part of this thesis discusses expansion on the previous work completed by Teague *et* al [16] to

create a more robust and convenient, low-cost method for obtaining and classifying knee joint acoustics with a wearable device as a potentially significant biomarker.

1.2 Cardiovascular Disease

In 2010, 82.6 million people in the United States suffered from one or more cardiovascular diseases (CVD) making it the leading cause of death nationally [17]. Chronic high blood pressure (BP), known as hypertension, has been clearly identified as a significant risk factor for all CVD including coronary heart disease, stroke, heart failure, aortic and peripheral arterial disease, and valvular heart disease [18]. While monitoring a patient's BP during clinic visits is an important step in identifying hypertension and CVD risk, blood pressure variability (BPV), short term changes in BP, has also been identified as a significant risk factor for CVD related mortality but is difficult to measure with current devices [19]. In order to track these short term changes, more continuous BP monitoring should be performed for at-risk persons.

The current "gold standard" for blood pressure measurement is intra-arterial pressure sensing, requiring the insertion of a pressure transducer into an artery via a catheter. Due to the invasive nature, this method is more commonly implemented during surgery and critical care situations [20]. A more commonly accepted method for acquiring blood pressure in the clinic is auscultation which is done using a stethoscope, an inflatable bladder, and a sphygmomanometer. Although this method is non-invasive, several challenges render it impractical for continuous or semi-continuous out-of-clinic monitoring: specialized training is required to perform the test, occlusion of an artery can cause discomfort to the subject, and the beat-to-beat BP measurement cannot be found.

Automated oscillometric devices are currently available on the market and are capable of providing sufficiently accurate BP measurements, but similar to the auscultation method, these devices require arterial occlusion and cannot provide continuous BP measurement. The use of any occlusive, cuff-based measurement technique has been known to cause discomfort, disturb sleep, and be cumbersome for daily use [21]; therefore, a cuffless BP measurement system is desired.

Most current research on cuffless BP measurement systems employ methods based on the extraction of pulse arrival time (PAT), the time interval between ventricular depolarization and the arrival of blood at a distal location, to estimate BP. These systems attempt to obtain proximal timing references via electrocardiogram (ECG) and distal timing references from pulse wave sensors such as photoplethysmogram (PPG) [22, 23], electrical bioimpedance (EBI) [24], or epidermal pulse (EP) [25]. While the PAT method has been found to correlate well in some studies with systolic blood pressure (SBP), the confounding effect of the pre-ejection period (PEP) motivates the need for true proximal timing references such as impedance cardiogram (ICG), ballistocardiogram (BCG), or seismocardiogram (SCG) instead of ECG [21, 26-30]. The time interval from this proximal timing to a distal timing event is then known as pulse transit time (PTT). The research outlined by Kim and Carek *et al* [26] found that PTT was better correlated with BP than PAT for calculating SBP, diastolic blood pressure (DBP), and mean arterial pressure (MAP), calculating r-values of 0.79 and 0.59 (DBP), 0.83 and 0.69 (MAP), and 0.84 and 0.75 (SBP) for PTT versus PAT respectively. Similar results were confirmed in other studies by Zhang *et al* [28], Geddes *et al* [29], and recently by Martin *et al* [31]. The second part of this thesis describes expansion on the previous work outlined by Kim and Carek *et*

al [26] to continue developing systems that utilize the PTT method of deriving beat-to-beat BP for continuous or semi-continuous out-of-clinic monitoring.

1.3 Research Goal

In addition to the fact that both proposed systems can aid in improving care for a number of cardiovascular and joint health complications, they could specifically improve quality and cost of care for CVD and arthritis in the growing aging population. Since CVD is the leading cause of death in adults over the age of 65, and more than 50% of this population suffers from arthritis, the goal of this research is to develop novel systems which will lessen the burden of these diseases on healthcare. Continuous, out-of-clinic monitoring may become increasingly necessary in helping healthcare specialists care more completely for a greater number of aging individuals simultaneously by making it possible to record and process out-of-clinic data.

CHAPTER 2. BACKGROUND

In the beginning of this chapter, relevant background information pertaining to the current OA assessment methods, their shortcomings, and the application of joint acoustics as a potential biomarker for OA will be presented. This is followed by a discussion of current BP measurement techniques, previous work on cuffless BP estimation via PTT, and the biomechanical signals explored in this document for use as proximal and distal PTT timing references. While both OA and hypertension can currently be monitored in-clinic, such infrequent monitoring does not provide a dynamic understanding of treatment effectiveness or condition variability which is essential to providing personalized care. With the use of low noise analog electronics and custom front end circuits, wearable systems for non-invasive monitoring of OA and BP can be realized to better serve the aging population.

2.1 Osteoarthritis Diagnosis and Monitoring

OA is the most common joint disorder without an approved treatment method currently identified [14]. Joint pain or loss of movement are often the first symptoms which lead to an individual being assessed for development of OA [8]. However, these effects are usually not noticed by the patient until the disease has already compromised joint integrity to the point that pharmacological treatments rarely impact the prognosis. Invasive arthroscopy, the "gold standard" for joint assessment, is not used for early arthritis monitoring because of the inherent risk of any surgical procedure, and commonly used imaging techniques such as X-ray are only able to detect changes in joint space or articular cartilage damage once they are significant [10, 32]. Therefore it would be beneficial to

identify bio-markers which can be used to detect the onset of OA earlier in the disease progression, and/or quantify treatment effectiveness so that early action, and/or treatment modification can be employed to improve the prognosis. Knee joint acoustics, have shown differences in time and frequency domain characteristics in arthritic subjects compared to normal knee acoustics during flexion and extension exercises[10, 33], and may prove to be a viable means of quantifying early onset and treatment assessment of OA.

2.1.1 Osteoarthritis Assessment with X-ray and MRI

During an examination for OA diagnosis, the clinician will passively induce movement in the joint of interest. Observance of crepitus or locking during such movement will suggest the presence of osteophytes, which are a primary symptom of OA. Plain radiography is then typically used to confirm the diagnosis. Although X-ray imaging can be used to quickly produce high-resolution images, the ability to quantitatively detect changes in joint condition based on this technique typically take at least a year since the expected annual joint space decrease due to OA is less than 0.15 mm, but the maximum resolution of current radiography technology and procedures is limited to 0.20 mm under ideal conditions [13, 14]. This level of accuracy requires many image angles, and between image positional standardization that is rarely applied in clinical settings [8]. Despite the fact that this procedure is unable to closely monitor the effects of treatment or disease progression, it is the only approved method of OA classification [14]. The semi-quantitative Kellgren and Lawrence grading system is the most widely used classification method, and applies a scoring system based on the presence of osteophytes and joint space narrowing; but is largely unable to distinguish disease progression [14].

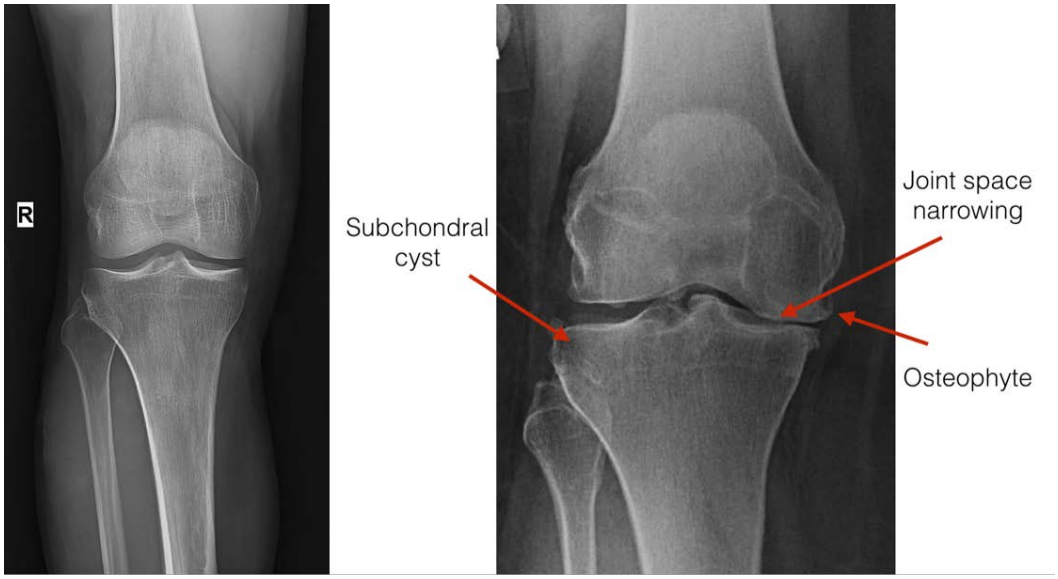

Figure 1: (A) An X-ray negative of a healthy knee can be easily distinguished from (B) an X-ray negative of an arthritic knee. In the arthritic knee the medial joint space compartment is severely narrowed, osteophytes (commonly called bone spurs) are present on the femoral condyles and patellar plateau, and a cyst has formed in the patella. (A) Open source image from [34]. (B) Used with permission from [35].

As a result of the highly accurate measurements which can be obtained using magnetic resonance imaging (MRI), this method better suited for quantitative analysis of OA. However, MRI is rarely used for clinical diagnostic or monitoring purposes because of the long procedure duration (~45 minutes) and high cost ($2,600 on average) [14]. In contrast, it is being used in OA research and provides a greater ability to identify osteophyte formation, accurate measurement of joint space narrowing, and assessment of soft tissue and cartilage integrity.

Figure 2: An MRI of the knee joint provides the ability to not only visualize the integrity of the bone, but also differentiate between soft tissues for assessment of synovial and meniscal tissue damage. Open source image from [36].

2.1.2 Exploring Joint Acoustics as a Biomarker for Osteoarthritis

Currently there are no available biomarkers apart from the aforementioned imaging techniques known to provide relevant information in regard to the diagnosis or prognosis of OA [8]. Therefore, because of X-ray radiology's shortcomings in accuracy, and MRI's duration time and high cost, finding an easily obtainable, affordable biomarker for OA diagnosis and monitoring is critical to developing a greater understanding of the effectiveness of treatments and early detection of the disease.

Joint acoustics have been investigated since 1902 but have yet to produce clinically acceptable results for joint health assessment [37]. However, recent studies by Kim *et al* [10, 33] have been able to demonstrate the ability to discriminate the more frequent, longer duration vibrations associated with crepitus in patients with OA apart from the less frequent, high frequency clicks present in healthy knees during flexion and extension for OA identification. Observed parameters in these studies include the fundamental frequency, jitter, shimmer, energy distribution, energy spread, frequency distribution, and frequency spread of knee vibrations between 0.02-2 kHz. However, work by Teague *et al* [16], and Toreyin *et al* [38] have shown that there are consistent clicks present in healthy subjects' knees at frequencies as high as 20 kHz during non-weight bearing flexion-extension and weight bearing sit-to-stand exercises. Therefore, investigation of a broader band of joint vibrations may further improve the ability to distinguish and quantify OA based on joint acoustics.

2.2 Blood Pressure Monitoring for Cardiovascular Health Evaluation

Hypertension is the most common risk factor assessed for estimation of cardiovascular health because of its strong correlation with all other CVDs including coronary heart disease, stroke, heart failure, aortic and peripheral arterial disease, and valvular heart disease [18]. Therefore, in order to more continuously monitor cardiovascular health in the aging population, more continuous blood pressure measurement data is needed to provide critical insight needed by today's clinicians. While monitoring a patient's BP during clinic visits is an important step in identifying hypertension and CVD risk, short term changes in BP, referred to as blood pressure variability (BPV), have also been identified as a significant risk factor for CVD related

mortality [19]. Automated BP extraction via oscillometry allows for out-of-clinic, semi-continuous assessment of blood pressure, but these devices are bulky and have been known to cause patient irritation due to the occlusive method of BP extraction [21]. In order to track these short term changes, without disturbing the individual's daily life, a more continuous, non-occlusive method of BP measurement should be developed for monitoring at-risk individuals.

2.2.1 Blood Pressure Measurement Methods

Intra-arterial blood pressure measurement is the gold standard blood pressure measurement technique due to its ability to provide continuous, direct, beat-to-beat blood pressure; thus making it the ideal procedure for patients in critical care situations [20]. The method for obtaining this measurement is invasive however, and requires the cannulation of an artery. The cannulation can result in thrombosis, emboli, ischemia, or infection in the patient and is only used in-clinic when semi-continuous non-invasive techniques such as auscultation and oscillometry are not adequate. Non-invasive blood pressure measurement can be taken by a medical professional through a common technique known as auscultation or by an automated oscillometric device. Both methods utilize an occlusive cuff which is inflated to a pressure above SBP and slowly drained to determine SBP and DBP. MAP can then be estimated by equation (1). The method of auscultation is widely accepted in practice and is used for comparison of other BP measurement modalities despite the fact that this method may at times compromise accuracy due to inter-observer variability and error [39].

(A) (B)

Figure 3: Traditional non-invasive methods are based on occlusive methods which require a bulky inflatable cuff. The auscultation method (A) requires a trained medical professional listening for Korotkoff sounds as cuff pressure decreases. While widely accepted, this method has been seen to suffer from inter-observer variability[39]. Automated oscillometric devices (B) also require an occlusive cuff. (A) Open source image from [40]. (B) Open source image from [41].

Oscillometry is primarily used for semi-continuous BP monitoring for hospitalized individuals and may also be used for at-home monitoring [42]. The main advantage of this method is elimination of the need for a trained professional to repeatedly perform the auscultation method on a patient. A calibrated oscillometric device is capable of producing BP measurements within 15 mm Hg of intra-arterial pressure at least 95% of the time [43], but have proved to be less accurate for patients with arrhythmias due to heart rate variability, or diabetes, renal failure, and peripheral arterial disease due to changes of arterial elasticity [42]. This poses a significant problem for using oscillometric devices for monitoring hypertensive patients who are prone to suffer from such comorbidities.

2.2.2 Non-invasive Cuffless Blood Pressure Measurement

In order to prevent the need of arterial occlusion, cuffless methods of non-invasive, automated blood pressure extraction have been investigated. A commonly referenced

surrogate indicator for non-invasive blood pressure estimation is pulse wave velocity (PWV) which can be related to blood pressure by the Bramwell-Hill equation (2), a modified version of the Moens-Korteweg equation (3).

$$PWV = \sqrt{\frac{A}{\rho \cdot C}} = \sqrt{\frac{dP \cdot A}{\rho \cdot dA}} \tag{2}$$

$$PWV = \sqrt{\frac{E \cdot h}{2 \cdot r \cdot \rho}} \tag{3}$$

Where C is the arterial compliance, P is the pulse pressure, A is the cross sectional area of a vessel, and ρ is the blood density in (2), and E is the elastic modulus of a vessel wall, h is the thickness of the wall, r is the vessel wall radius, and ρ is the blood density in (3). Since PTT is directly related to the length of blood travel, l, and PWV by (4) it can also be related to pulse pressure by substituting (4) and (5) into (2) yielding (7), or (4) and (6) into (3) yielding (8).

$$PTT = \frac{l}{PWV} \tag{4}$$

$$C(P) = \frac{dA}{dP} = \frac{A_m}{\pi P_1 \left[1 + \left(\frac{P - P_0}{P_1}\right)^2\right]} \tag{5}$$

$$E(P) = E_0 e^{\alpha P} \tag{6}$$

(2), (4), and (5) yield: $$BP = \frac{K_1}{PTT} + K_2 \quad (7)$$

Or (3), (4), and (6) yield: $$BP = K_1 \, ln(PTT) + K_2 \quad (8)$$

Where K_1 and K_2 are unknown subject dependent variables that must be initially calibrated and periodically recalibrated to account for physiological changes such as age related arterial stiffening [44].

Many current cuffless blood pressure estimations use the R-peak of an ECG QRS complex as a proximal timing reference [22, 23, 25]. This is due to the fact that the ECG signal is robust, well understood, and easily acquired bio-potential signal [30]. However, the ECG R-peak value corresponds to ventricular depolarization which proceeds ventricular ejection. The time delay between ventricular depolarization and ejection is known as PEP and corresponds to the isovolumetric contraction portion of systole. The problem with including the PEP timing interval for BP estimation is that PEP can be influenced by decreased pre-load, increased aortic pressure, or changes in contractility, and can negatively correlate with changes in blood pressure [28]. When using ECG as the proximal timing reference it is therefore PAT, not PTT, being measured and the pulse propagation time can be influenced by changes in PEP by 10-35% [28].

Current PTT based BP technologies employ a number of different sensing modalities to capture the timing references; for a detailed review of each, and PTT based BP estimation overall, the reader is referred to [30]. The particular sensing modalities for PTT used in this work were BCG or SCG (as a proximal timing reference) and PPG (as the

distal reference). These are discussed below. ICG, which was used for evaluation of BCG and SCG performance as a proximal timing reference is also discussed.

2.2.2.1 Impedance Cardiogram as a Proximal Timing Reference

ICG, a form of EBI, is most commonly used for a non-invasive measurement of stroke volume, but is also the standard method for non-invasive detection of aortic valve opening [30]. The B-point, seen in figure 4, represents the opening of the aortic valve and can therefore be used as a proximal timing reference for PTT calculation. Multiple factors can negatively affect EBI/ICG signal quality such as obesity, respiration, and movement [45]. A thicker layer of subdermal fat will result in an increased baseline thoracic impedance, and will also affect the changes in impedance caused by the influx of blood into the aorta [46]. While respiratory and motion artifacts can be mitigated or filtered for improved EBI/ICG accuracy, obesity cannot be mitigated and is a common comorbidity in hypertensive and pre-hypertensive individuals; thus reducing the robustness of this measurement technique for cuffless blood pressure estimation in the target population.

2.2.2.2 Ballistocardiogram as a Proximal Timing Reference

BCG is a measurement of the reactionary forces of the body to the acceleration of blood being ejected from the left ventricle into the ascending aorta, and the subsequent movement of blood through the arterial tree. The maximum amplitude of the BCG signal can be as small as 1-7 m*g* but is sufficient to be measured by many commercially available accelerometers, strain gauges, and load cells integrated into bathroom scales, hospital beds, chairs, and wrist worn devices [47, 48]. Of the H-, I-, and J-waves which can be observed in the BCG signal shown in figure 4, the I-wave is used for the proximal timing reference

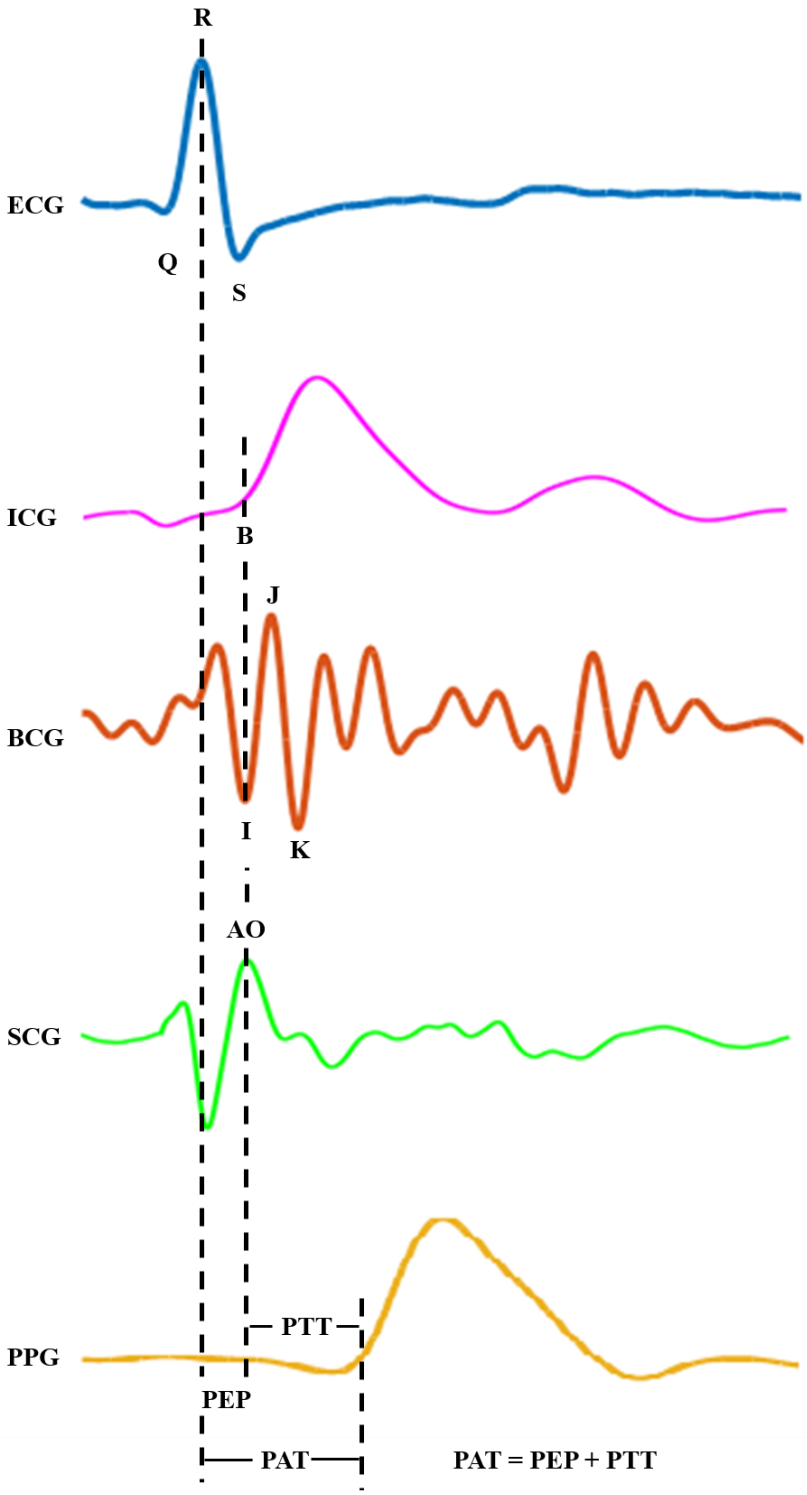

Figure 4: ICG, BCG, and SCG can serve as proximal timing references for PTT calculation. When ECG is implemented as the proximal timing reference the result is PAT which includes the PEP. Names of pertinent waveform features are shown**.**

as it has been associated with aortic valve opening based on a recently published model of the mechanism of the BCG signal [31]. The movement associated with BCG can be seen in all three anatomical planes, but the longitudinal displacement (head-to-foot) is the most commonly studied signal. The largest obstacle encountered when using BCG as a proximal timing reference for BP estimation are subject motion artifacts occurring during measurements. The BCG signal bandwidth range is limited from dc-40 Hz and should be bandpass filtered in both hardware and software to remove motion from the signal to the extent possible.

2.2.2.3 Seismocardiogram as a Proximal Timing Reference

SCG is the signal corresponding to the motion of the chest wall during the cardiac cycle and is sensed by simply placing an accelerometer against the chest to monitor the vibrations [47, 49]. Both the cardiac and pulmonary cycles will cause motion of the chest wall, but the motion resulting from the pulmonary cycle is at a much lower frequency than the cardiac related vibration and can readily be filtered from the signal. As can be seen in figure 5, the SCG waveform can be used to determine the time of aortic valve opening and can therefore serve as a proximal timing reference for PTT measurement. Preliminary studies have used the aortic valve opening feature found in SCG as the proximal timing reference, but rapid ejection may also be sufficient [27]. It should be investigated as to which timing reference correlates more strongly with changes in BP.

2.2.2.4 Photoplethysmogram as a Distal Timing Reference

PPG sensors are used clinically to non-invasively monitor the oxygen-hemoglobin saturation of pulsatile blood (SpO2), and can also be used to determine other cardiovascular

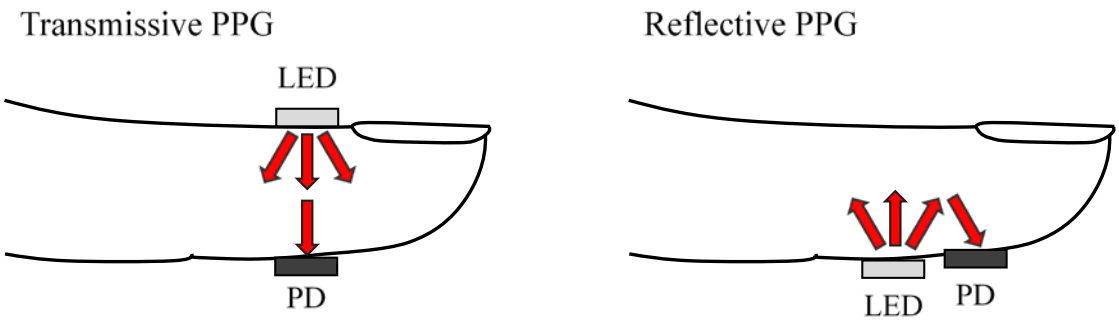

Figure 5: The PPG signal can be detected in either the transmissive or reflective mode. The change in emitted LED energy delivered to the photodiode is caused by the changes in blood volume due to the high absorption rate of hemoglobin. In addition to pulse detection, PPG can be used to detect heart rate, respiration rate, and transmissive PPG using a combination of IR and red LEDs can be used for SpO_2.

features such as heart rate and change in pulsatile blood volume in a given tissue location. PPG can be measured by using a combination of one or more light-emitting diodes (LEDs) with one or more photodiodes (PDs) in either transmissive or reflective orientation. The intensity of light captured at the PDs is therefore a measurement of the amount of light transmitted through or reflected back from the illuminated tissue. While the dc component of the PPG signal is based on the structural makeup of the illuminated tissue, the ac component is able to provide information about changes in blood volume in the illuminated area because of the Beer-Lambert law for light absorption in a given medium given by equation (9) [30].

$$ln\left(\frac{I(t)}{I_0}\right) = -\varepsilon \cdot C \cdot V \tag{9}$$

Where I(t) is the intensity of light transmitted through the medium, I_0 is the intensity of the source, ε is the absorption coefficient of the medium, C is the concentration of the chromophore, and V is the volume. Since hemoglobin is highly absorptive to the wavelengths of light used in PPG sensors, an increase in blood volume in the illuminated area causes less light to be either reflected or transmitted through the tissue which can be used to find heart rate or pulse volume.

To use PPG as a timing reference for PTT calculation, either green, red, or IR LEDs can be used. Because green has the shortest wavelength it is more robust to motion artifacts, but is unable to penetrate past skin depth [50]. Since changes in the microvasculature of the skin can be dramatically affected by temperature, it is not recommended to use a green LED for PTT timing reference. In addition, transmission mode PPG is limited by the penetration depth of the LED and is only usable at distal sites including the fingers, toes, or earlobe where blood flow is also more sensitive to environmental temperature and neural modulation than larger arteries, making reflectance mode PPG more suitable for PTT timing reference determination at sites including the wrist, dorsum of the foot, or forehead [30]. PPG can be negatively affected by motion artifacts and changes in contact pressure during measurement, but is a high quality and commonly used method for cuffless BP distal timing reference.

CHAPTER 3. DESIGN, SIGNAL PROCESSING, AND METHODS

3.1 Joint Sound Recording Instrumentation and Physical Design

This project began with improving the previously used joint sound recording system [16] performance by implementing the system in a wearable, untethered design and improving the measurement methods by creating an ultra-low noise AFE pre-amplifier. The joint sound recording system will be designed to record joint sound data using two piezo-ceramic contact microphones, BU-23173, as well as joint angle data from two digital three axis accelerometer & gyroscope IMUs, LSM6DS3, corresponding to the acoustical emissions of the knee. A block diagram of the system architecture can be seen in figure 6.

3.1.1 Analog Front End Design for Joint Sound Recording

In order to obtain high quality acoustical signals from the knee joint with the contact microphone, an AFE was designed for low noise amplification and filtering of the output signal. Radio frequency interference (RFI) and DC offset is removed from the signal before the gain stage of the AFE by use of a second order 8 MHz LPF cascaded to a 0.159 Hz first order high pass filter (HPF). The following gain stage has a manually selectable gain, operated by a single pole double throw (SPDT) switch, of 20 or 40 dB with a 16 Hz HPF on the output. The last stage of the AFE includes a 6^{th} order Butterworth 20 kHz LPF in a Sallen-Key topography with unity gain and RFI filtering added at the output.

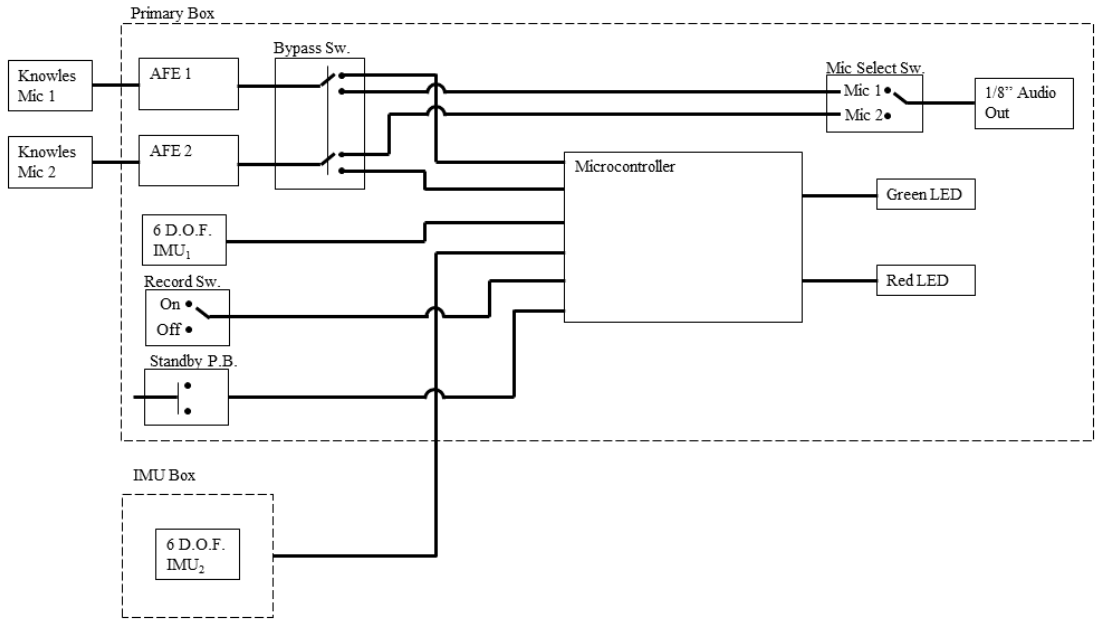

Figure 6: Block diagram of the joint sound recording system architecture which is comprised of two electronics boxes and two Knowles contact microphones.

When designing the front end, the IC selection played a critical role in fulfilling the ultra-low noise requirement for the given application. The amplifier used in the gain stage of the AFE is an LTC6240 (Linear Technology, Milpitas, California) with an 18 MHz gain bandwidth product (GBWP). Therefore, even at the voltage gain setting of 100, the amplifier can support a 180 kHz bandwidth, nine times greater than the filter cutoff frequency in the front end. In addition, the IC has a mere 7 nV/$\sqrt{\text{Hz}}$ resulting in ~1 μV_{RMS} in band noise at the input, and ~100 μV_{RMS} at the output. The LTC6257 used in the filter stage has a 20 nV/$\sqrt{\text{Hz}}$ noise per amplifier, resulting in an added ~8.5 μV_{RMS} at the output for a calculated total of 108.5 μV_{RMS} with the chosen ICs.

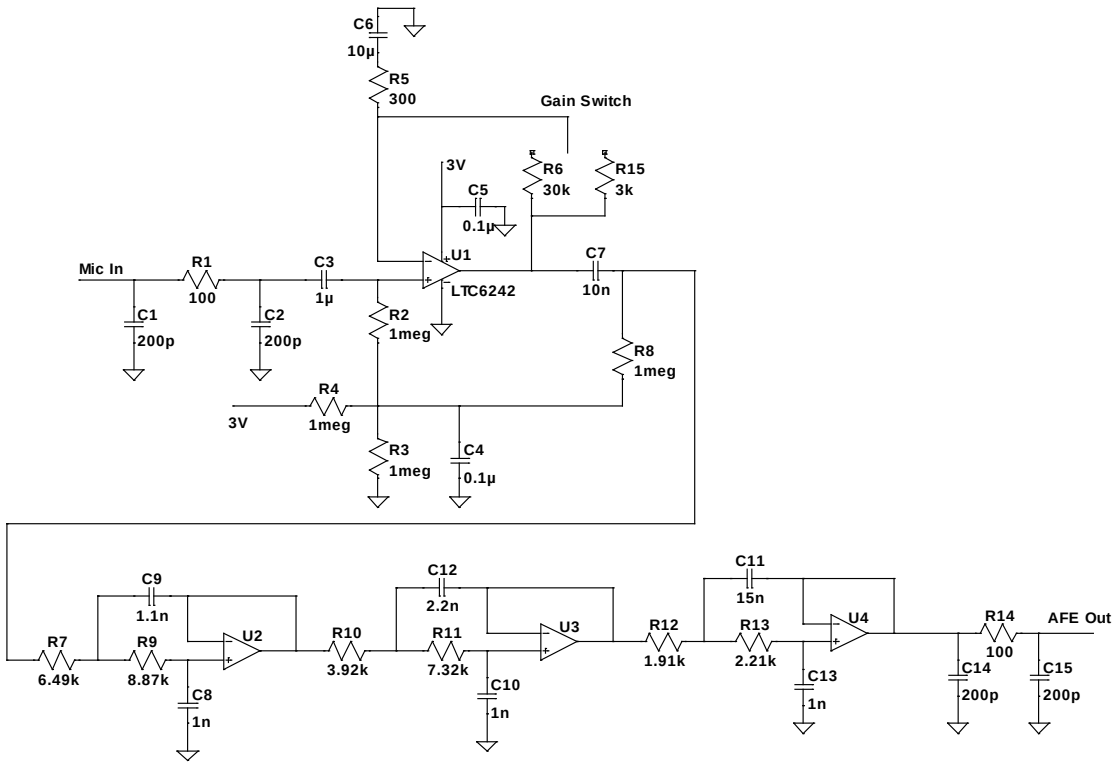

Figure 7: The circuit schematic containing the gain and filter stage design of the AFE. Not shown in the diagram is the voltage regulator IC which sets the 3 V output used for powering the amplifiers and microphone, as well as set the midpoint voltage used to bias the input signal in the single supply design.

The AFE was created in LTSpice (Linear Technology, Milpitas, California) and simulated for verification of design. Once the design was confirmed, a PCB board layout was designed using EAGLE (CadSoft, Guelph, Ontario) to develop a set of Gerber files. All of the resistors and capacitors, except for the 10µF tantalum capacitors, were selected to be 0402 surface mount package and the 10µF tantalum capacitors were selected to be 0603. Once the PCB was assembled, the AFE pre-amplifiers were characterized using a SR785 Dynamic Signal Analyzer (Stanford Research, Stanford, California). The characterization included frequency response, total harmonic distortion, dynamic range,

step response, and noise floor of the AFE. The results from the characterization can be seen in Chapter IV.

3.1.2 Wearable System Implementation

The primary electronics box is a Bud Industries (Willoughby, Ohio) CU-341-A and houses the STM32F405 microcontroller board, the accompanying breakout board connected via 32 conductor flex cable, two microphone pre-amplifier circuits, one 6-degree of freedom IMU, and one 850 mAh polymer lithium ion battery (figure 8.A). The front panel of the primary box includes two TB3M XLR connectors for connecting to the microphones, one TB6M XLR connector for connecting to the IMU box, one green LED for power up and data recording notification, one red LED for recording error notification, one momentary pushbutton for toggling the microcontroller in and out of standby mode, one single pole slide switch for data recording start and stop, and one double pole slide switch for controlling the destination of the microphone data (figure 8.C). During data collection, the microphone data must be directed to the microcontroller from the pre-amplifier circuits; however, it may be beneficial for the investigator to have the ability to bypass the microphones and directly listen to the microphones. This bypass ability can aid in determining optimal microphone placement thereby improving the system performance. When placed in the “bypass” position the double pole switch can direct both pre-amplifier signals to a single pole slide switch located on the back panel of the primary box. This single pole slide switch is used to route the signal from the individual pre-amplifiers to a 1/8” four conductor female audio connector also located on the back panel (figure 8.D). The IMU box, a Hammond Manufacturing (Guelph, Ontario) 1590LLB, contains the

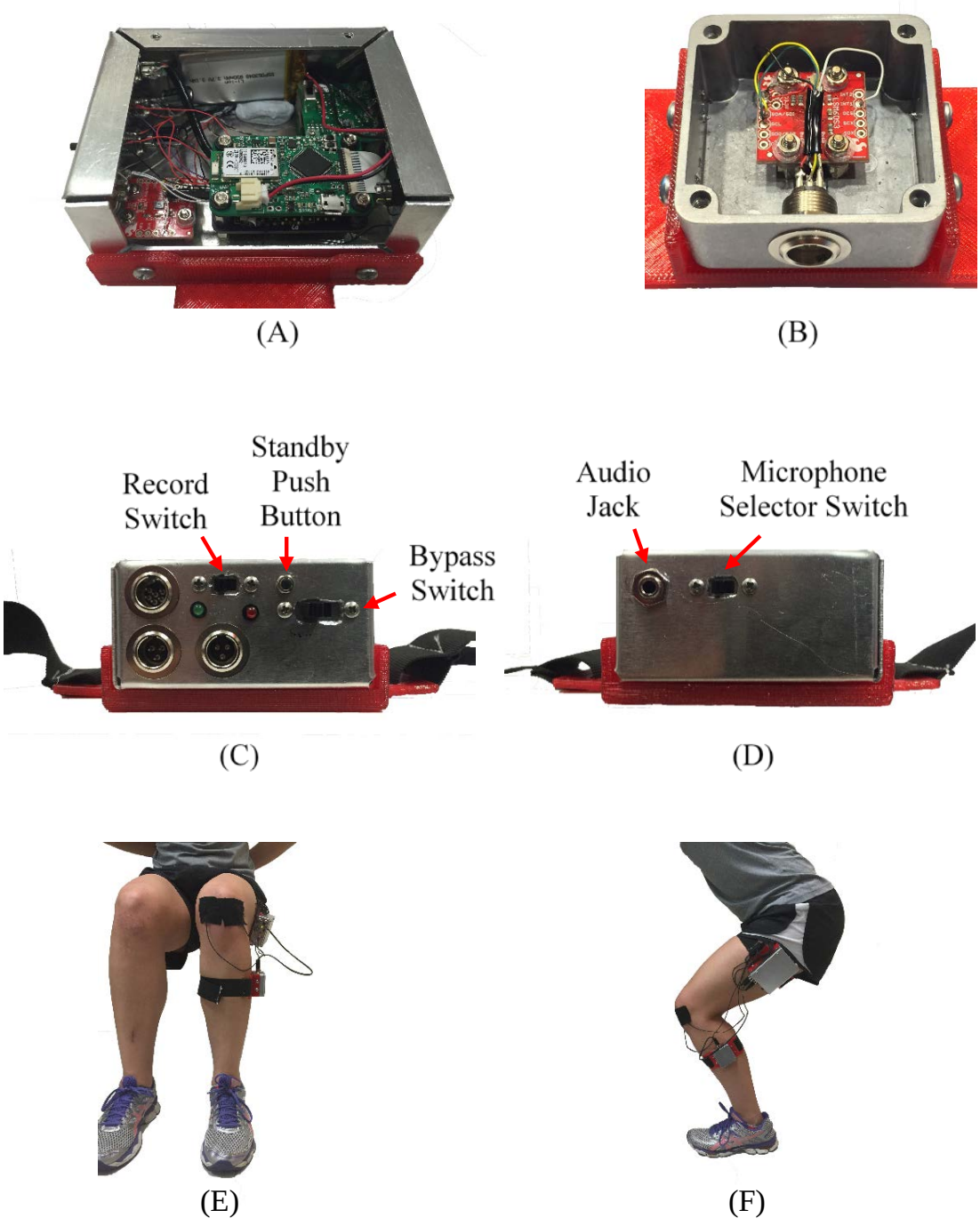

Figure 8: An image of the primary electronics box (A), IMU box (B), primary box front panel (C), and primary box rear panel (D). Also shown is a front view (E) and side view (F) of the system being worn for untethered joint sound recording during complex movements.

second 6- degree of freedom IMU (figure 8.B). The front panel of the IMU box includes one TB6M XLR connector for connecting to the primary box.

In order to interface with the subject, flexible mounting units were created to attach the primary box to the lateral side of the subject's thigh and the IMU box to the lateral side of the subject's shank. The straps used to suspend each mounting unit were created using Stretchrite 1-1/2" heavy stretch elastic knit and a Strapworks 1-1/2" plastic slide. The mounting units were printed in Ninjaflex flexible filament from NinjaTek. This wearable system can be used for untethered joint sound recording for studies during complex (e.g. pivoting, stair climbing, etc.) movements to analyze knee joint sounds in healthy and injured knees.

3.2 Cuffless Blood Pressure Design, Signal Processing, and Methods

3.2.1 Utilizing BCG and PPG for PTT Timing References

Work on the cuffless BP measurement system began by assisting A. Carek to assemble a modified bathroom scale prototype for measuring PTT. This device was similar to the system previously described by our group in [26]; however, in addition to measuring BCG as a proximal timing reference, the new prototype also included a Velcro foot-strap utilizing a single reflective PPG sensor to measure a distal pulse timing reference from the dorsalis pedis artery. With correct sensor placement, PTT could be captured as the time delay between the BCG I-wave and the foot of the arriving pulse waveform measured at the distal PPG sensor.

3.2.1.1 Modified Bathroom Scale to Measure BCG

BCG was measured using a modified weighing scale as seen in [51]. Four load cells at each corner of the scale are configured as a Wheatstone bridge. The scale used for the measurement is a BC-534 InnerScan Body Composition Monitor (Tanita, Arlington Heights, Illinois). The custom AFE used in the design inputs the differential voltage across the bridge to an instrumentation amplifier with a 54 dB gain, followed by a 0.5-24 Hz fourth order bandpass filter and a 35.5 dB gain [51].

3.2.1.2 Modified PPG Sensor Array

A key limitation of the design was that by only using a single PPG sensor the distal measurement was sensitive to placement error, and the sensor would often need to be moved several times before a reliable distal pulse waveform could be captured. This issue would likely be accentuated if the device were to be used by an individual unfamiliar with the anatomical structure of the foot. Therefore, in order to improve the robustness of the distal pulse detection despite variations in sensor placement or user knowledge of foot anatomy, as well as account for anatomical differences between individual users, an array of PPG sensors was constructed. The new sensor included an array of three PPG sensors incorporated into a sandal with an adjustable foot strap as seen in figure 9.A. In addition to modification of the PPG sensor design, a software program was created to process the output of each PPG sensor in the array and classify waveform as either high or low quality. Once classified, only high quality signals would be used to constitute the distal waveform for beat-to-beat PTT calculation.

The improved distal PPG sensor array was designed using a combination of three PPG sensors as seen in figure 9.A. The array utilizes a single 5 V line to reverse bias three photodiodes per sensor (S2386-18k, Hamamatsu Photonics, Shizuoka, Japan), placing the diode in the photoconductive mode, and to power the one red LED per sensor (L6112-02, Hamamatsu Photonics). This diode was selected due to its extremely low dark current of a maximum of 2 pA when a 10 mV reverse bias voltage is applied. The connected anodes of the three photodiodes in each PPG sensor are connected to the input of an individual channel of a custom AFE created by A. Carek (figure 9.B). Aligning the three photodiodes in parallel sums the currents together, reducing zero-mean noise. Each photodiode is photosensitive at a rate of 0.6 A/W of delivered energy. The current generated by each sensor channel is wired on the printed circuit board (PCB) to the negative terminal of an LT1678 (Linear Technology, Milpitas, California) which is arranged as a transimpedance amplifier (TIA). The AFE includes a 300 kΩ resistor in parallel with a 68nF capacitor for each TIA feedback loop. The resistor sets the transimpedance gain and dynamic range of the amplifier while the capacitor is used to reduce the gain of any out of band frequency feedback from the op amp which may result in oscillation; the passband cutoff of the RC feedback is ~8 Hz. Since the TIA is powered with a 5 V single supply, and the signal is referenced to a midpoint voltage of 2.5 V, the 300 kΩ resistor will cause the TIA to rail at currents exceeding ±8.33 µA. The voltage output of the TIA is then filtered through a filter stage which employs a two stage filter with 60 dB gain made up of an inverting bandpass filter in the first stage followed by a non-inverting Sallen-Key bandpass both with a ~0.8-8 Hz passband. The total TIA gain is 170 dB.

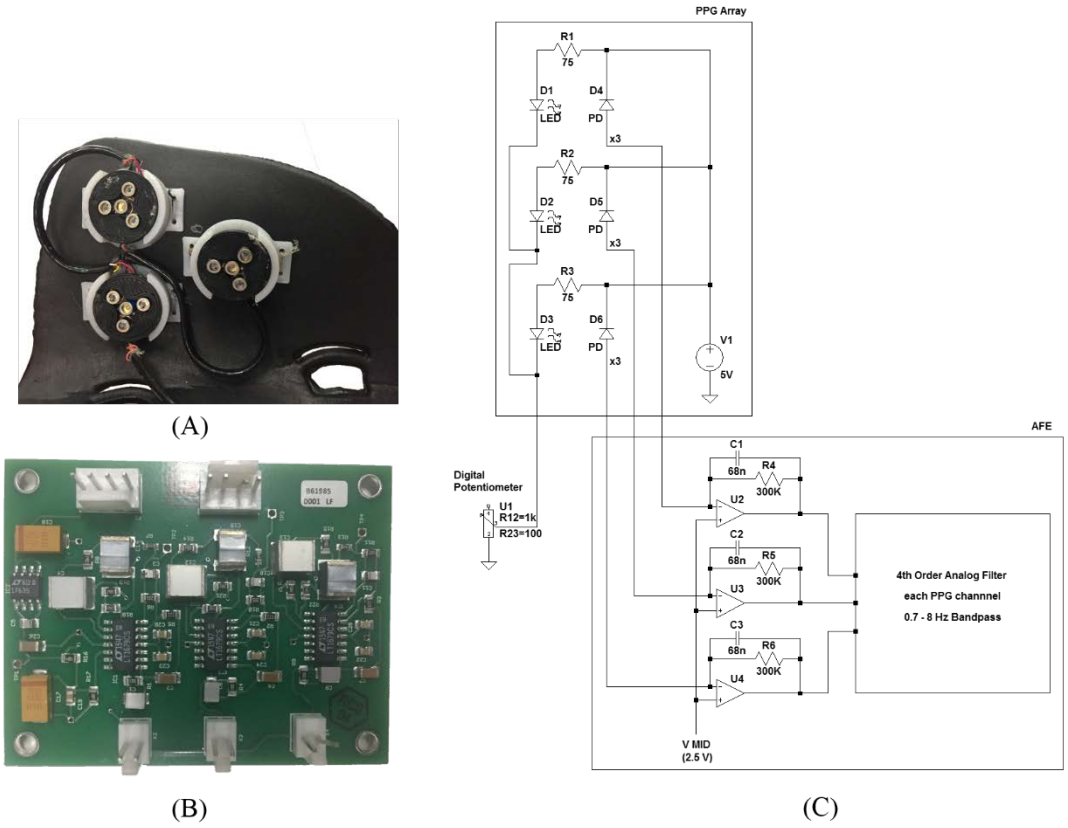

Figure 9: (A) The improved PPG array integrated into an adjustable Velcro sandal strap including 3D printed mounting fixtures for the LEDs and photodiodes in each sensor. (B) The PPG AFE developed by A. Carek. (C) The circuit schematic for the PPG array including the array, AFE, and digital potentiometer.

The L6112-02 LEDs used in the PPG sensors have a typical forward voltage drop of 1.8 V and produces a radiant flux of 2.5 mW with a 20 mA excitation current. Due to anatomical differences between the thickness and makeup of subdermal tissue between subjects' feet, the amount of light produced by a LED can negatively affect the output PPG signal, even when placed in the correct location, by either causing oversaturation of the photodiode TIA or not producing enough energy to obtain a defined pulse waveform from reflected light. Therefore, a digital potentiometer was added in series with the three parallel LEDs. This feature enables an easily adjustable control of the amount of current drawn

through the LEDs between data acquisitions. The series combination of the selected potentiometer, X9C102S (Intersil, Milpitas, California), and the 75 Ω input resistor to each LED have a total resistance range from 85-1075 Ω. With this range of resistance, current through each LED can be modulated between 3 and 38 mA. Therefore, the power consumption of each LED can range from 5.4 to 68.4 mW, allowing for simultaneous optimization of the system's power consumption and signal quality.

3.2.2 Quality Classification of PPG Signals

Upon testing the improved PPG sensor array, it was quickly discovered that the difference in position of the three sensors commonly resulted in a non-ideal placement of at least one sensor no matter where the array was positioned. The noise generated from the misplaced sensor tended to dominate the physiological signal, deteriorating the signal-to-noise ratio and making distal timing extraction difficult. Therefore, it was deemed desirable to be able to automatically determine the quality of a PPG signal detected from a particular sensor, and exclude any sensor data with a low-quality output. A classification algorithm was created using supervised machine learning based on features extracted from data taken using the PPG array.

3.2.2.1 Data Collection for Test-Set

Six-minute long recordings of PPG waveforms were collected from three subjects using the PPG array placed on the dorsum of each subject's right foot. Each PPG sensor in the array was connected to a channel of the custom AFE. The output of each channel was sampled at 2 kHz using three analog input channels of a BIOPAC MP150 (BIOPAC Systems Inc., Goleta, California) UIM100C universal interface module with the associated

AcqKnowledge 4.2 data acquisition and analysis software. At the conclusion of each six-minute recording, the data was saved as a MATLAB (MathWorks, Natick, Massachusetts) data file (.mat). During the recordings, two of the subjects were instructed to stand in a still position in an attempt to reduce motion artifact corruption of the signals. One subject was instructed to sway for twenty seconds of the recording. Each of the recordings was then parsed into four-second long intervals and plotted using MATLAB. By visual inspection, each of the 270 four-second long recordings was classified as either high-quality (1) or low-quality (-1). The high quality PPG signals appear as periodic waveforms with minute variation between each beat with a clearly distinguishable foot and peak of each arriving pulse. Additionally, the foot and peak amplitudes are consistent from beat-to-beat and the signal is not clipped by the supply rails. After the recordings were classified, the classification values were stored in a vector and used to develop a supervised learning model for PPG quality classification.

3.2.2.2 Feature Extraction

In collaboration with A. Carek, time and frequency domain features were then extracted to be used in the supervised learning process. Forty-five features were created in four different LabVIEW virtual instruments (VIs). A LabVIEW VI was then created by A. Carek to produce a spreadsheet of all forty-five feature outputs based on the 270 recordings. A supervised logistic regression with ten-fold cross-validation was performed on the extracted feature data using Weka (The University of Waikato, Hamilton, New Zealand), a logistic regression modeling program, and the classification vector. A ranked search was used to evaluate the features based on each feature's ability to predict correct

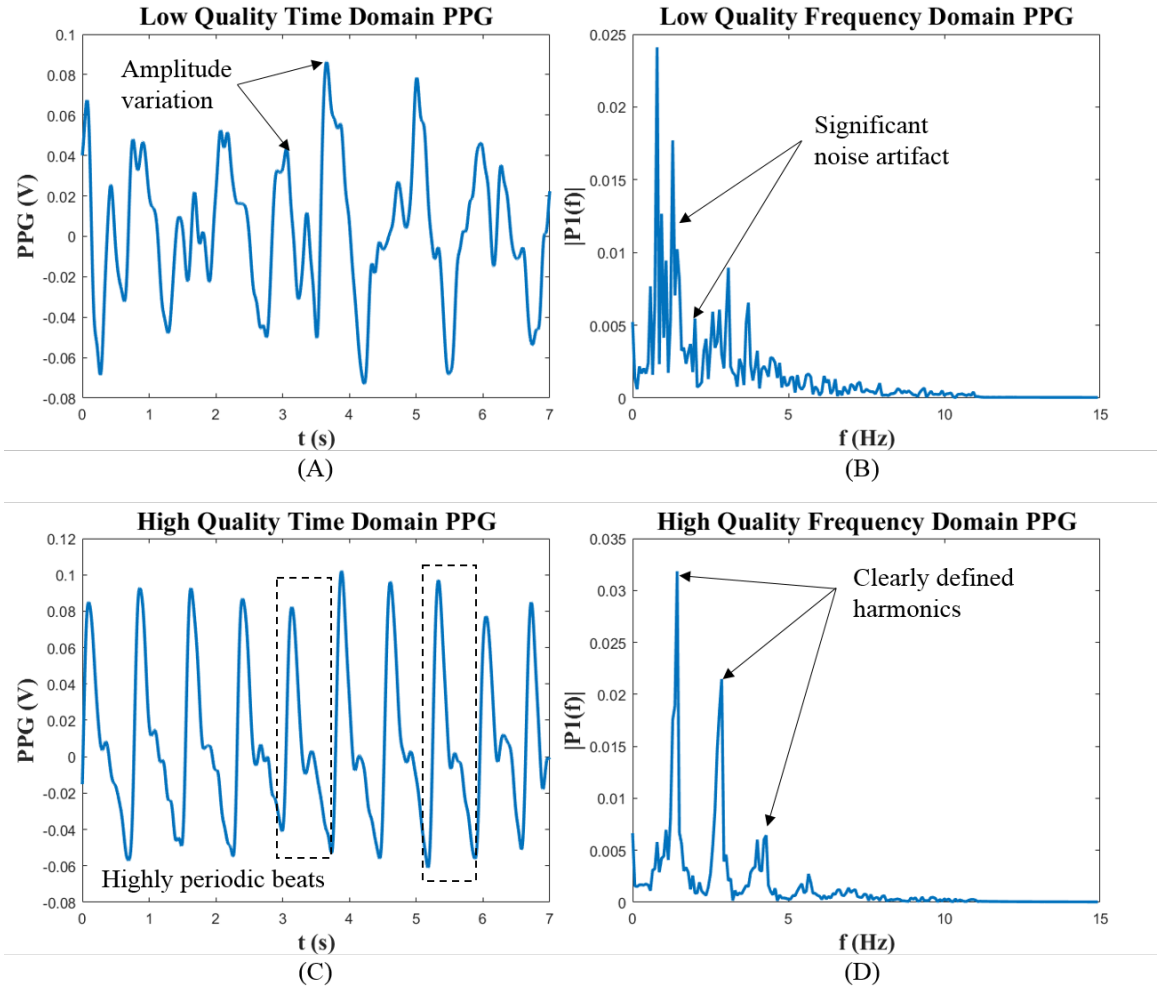

Figure 10: Example of a time (A) and frequency (B) domain PPG recordings of a low-quality PPG signal due to poor sensor placement. A high-quality time (C) and frequency (D) PPG signal includes more consistent peak height, periodic peak timing, and clearly defined frequency harmonics due to the periodicity of the signal.

classification of the test set [52]. It was determined that lowest performing features were overfitting the model and were therefore removed from the regression. This process was repeated until the removal of the lowest performing feature no longer improved the performance of the classifier on the test set. A total of eleven features were removed, leaving thirty-four features to be used in the development of the classification coefficients

and bias. The performance of the PPG quality classification algorithm is detailed in Chapter IV.

3.2.2.3 User Interface

The finalized classification coefficients were added into an array in the LabVIEW VI which incorporates a user interface (UI) design, the feature extraction, and classification of the PPG signals. The VI was implemented on a myRIO embedded hardware device, to which the BCG scale output and PPG sensor array outputs were connected. Upon receiving the start command from the UI front panel, four-seconds of PPG data is recorded simultaneously from each of the three PPG inputs. The feature extraction VIs would then calculate the thirty-four features from each PPG channel sample and store them in separate arrays. Next the classification coefficients were applied to the extracted features and the bias was removed. The sign of each result determines the signal classification, with a negative output representing the detection of a high-quality signal, and positive representing a low-quality signal.

The user was informed if no quality PPG signals were obtained during the initial sample, and another four-second sample would immediately be taken from the sensors for re-evaluation. If PPG signals remained low-quality for several evaluations, the PPG strap pressure and position could be adjusted until a quality signal was found. If one or more quality signals were obtained during the four-second recording sample, the VI would begin plotting the real time recording of PPG and BCG signals in separate plots on the user interface. The output PPG data plotted would be the sum of the high-quality PPG waveforms. At this point, the recording could be stopped at any time and cursors on the

plots could be manually positioned at the I-wave of the BCG signal and the foot of the PPG pulse wave of the same beat. The time difference between these two references represents the PTT associated with that beat. PTT could similarly be calculated for each beat in the recording which would allow for continuous beat-to-beat estimation of blood pressure based on equation (8). Values of K_1 and K_2 need to be calibrated for each individual for the estimation.

3.2.3 Seismocardiogram Implemented as a Proximal Timing Reference

Although the BCG-PPG based system is capable of continuously measuring beat-to-beat PTT and, therefore, allows for estimation of beat-to-beat BP, design improvements were desired to realize a wearable system implementation of PTT measurement. It was decided that SCG would be pursued as a proximal timing reference in a watch based system, with a wrist based PPG implemented into the backside of the watch face as a distal timing reference.

3.2.3.1 Accelerometer Selection

A low noise accelerometer, LIS344ALH (STMicroelectronics, Geneva, Switzerland), was chosen to measure the chest wall vibrations which compose the SCG signal. The accelerometer has a sufficiently low noise density level of 50 $\mu g/\sqrt{\text{Hz}}$ for the SCG measurement. On each axis of the accelerometer a 110 kΩ output resistor is in series with the output signal inside the device. A single pole low pass filter with a cutoff frequency of ~66 Hz was implemented at the Z-axis output by adding a 22 nF capacitor to ground. With this bandwidth, and a single pole low pass filter (LPF), the approximate RMS noise of the sensor can be calculated as seen in equation (10). The peak-to-peak

noise can then be assumed to be within 6.6 standard deviations of the RMS noise 99.9% of the time (11).

$$N_{RMS} \cong \ 1.57 \cdot N_0 \cdot \sqrt{BW} \tag{10}$$

$$N_{P-P} \cong \ 6.6 \cdot N_{RMS} \tag{11}$$

This results in a 4.2 m$g_{p\text{-}p}$ referred to the input (RTI) sensor noise; one-fifth of the expected 20 m$g_{p\text{-}p}$ SCG vibrations. In addition, when powered by a 3 V source the accelerometer has a 0.6 V/G sensitivity. Therefore, the expected output will be 12 m$V_{p\text{-}p}$, which can be sufficiently measured by the 16-bit, ±10 V ADC in the BIOPAC MP150 which has a 0.3 mV specificity.

3.2.3.2 Proof of Concept

Testing was performed to determine the feasibility of using the LIS344ALH accelerometer for SCG detection. The preliminary tests included characterization of the robustness of the sensor measurement against differences in contact pressure between the sensor and the sternum, as well as robustness against user placement error by taking SCG measurements at different locations along the sternum and thoracic cage. All studies were approved by the Georgia Institute of Technology Institutional Review Board.

To characterize the measurement robustness against contact pressure and placement error, four subjects were recruited and SCG data was recorded from each subject with the LIS344ALH accelerometer. A FS20-0000-1500-G (Measurement Specialties, Hampton, Virginia) low force compression load cell was used to determine effects of

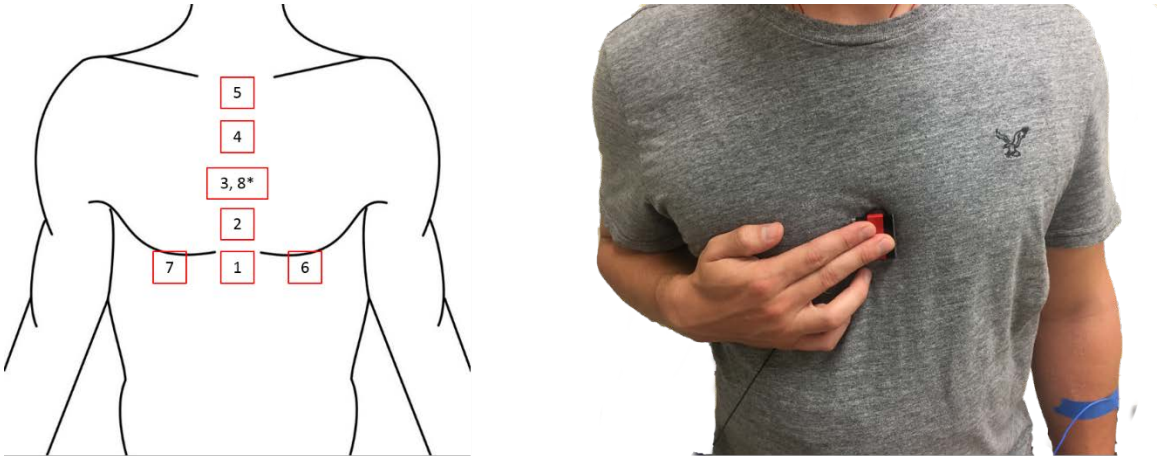

(A) (B)

Figure 11: (A) The eight positions used to test the robustness of the SCG measurement to placement error. Positions 1-3, and 8 produced consistent results for PEP extraction between the subjects. (B) An example of the robustness test with the load cell pressed into the accelerometer which was placed against the chest at each position.

contact pressure by measuring the applied force the subject exerted on the accelerometer as it was positioned on the sternum. To evaluate positional placement effects, SCG was recorded from seven different positions over a thin article of clothing (e.g. a t-shirt) between the accelerometer and the skin: position one located at the xiphoid process, position five being slightly inferior to the suprasternal notch, and positions two, three, and four evenly spaced between them as seen in figure 11.A. Position six was eight to ten centimeters left of position one, and position seven eight to ten centimeters right of position one. Finally an eighth recording was taken at position three except this recording was taken with the accelerometer making direct contact with the skin (i.e. clothing article removed). At each position, SCG was recorded using BIOPAC MP150 UIM100C and associated AcqKnowledge data acquisition software for three twenty-second intervals at the specified force gradient. With the load cell placed on the back of the accelerometer, subjects were

asked to hold the accelerometer in place by exerting forces of 125, 375, and 625 grams, correlating to a light, median, and hard press (figure 20). In addition to SCG, ECG was recorded using the BIOPAC BioNomadix 3-lead wireless ECG transmitter. All data was saved as MATLAB data files for processing.

First, each set of recorded data was parsed into beats using the ECG R-peak as the starting reference of each beat by R-peak detection algorithm. Once each beat had been parsed, the aortic opening (AO) feature of the SCG signal was extracted from each beat. For each subject, the R-peak of the ECG to the AO of the SCG (R-AO) interval was compared between each of the eight evaluated positions and between each of the applied pressures. The results of this comparison are detailed in Chapter IV.

3.2.3.3 Extracting PEP with a Watch Based Prototype

In addition to characterizing SCG robustness in the proof of concept study, the accuracy with which the watch-based SCG prototype could capture the AO point was assessed. Specifically, PEP (R-AO) measurements using the SCG based system were compared with simultaneously recorded results from the ICG (R-B). Since it is well documented that PPG can serve as a distal timing reference for PTT, a strong correlation between SCG and ICG would provide an important step towards validating the system's use for obtaining quality PTT measurement. A watch based prototype was developed using the LIS344ALH accelerometer inserted into the 3D printed watch face for SCG measurement, and two IR LEDs, VSMF2893GX01 (Vishay Intertechnology, Malvern, Pennsylvania), combined with two S2386-18k photodiodes for PPG measurement at the

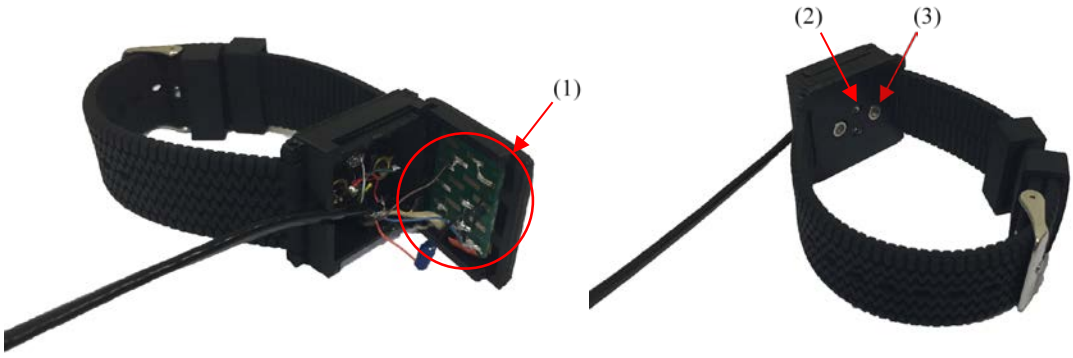

Figure 12: The watch prototype including the LIS344ALH low noise accelerometer (1), the VSMF2893GX01 IR LEDs (2), and the S2386-18k photodiodes (3) used to detect SCG-PPG based PTT for blood pressure estimation. The current prototype is implemented in a wired setup.

palmar side of the wrist. The prototype PPG output was wired to the PPG AFE described previously, and the Z-axis of the SCG measurement was wired to a perforated board and stabilized across a 10 nF capacitor to ground. In addition, the wires in the cable were shielded to reduce any RFI. The finished prototype can be seen in figure 12.

Three subjects were recruited and measurements were taken from positions 1-3 (positions described in the previous study) using the prototype by firmly pressing the watch face against the sternum at the specified locations. SCG and PPG signals measured using BIOPAC analog input channels. ECG and ICG were also recorded during the study using BioNomadix 3-lead wireless ECG transmitter and BioNomadix wireless NICO (non-invasive cardiac output) 8-lead ICG transmitter. Data collection from each position began with the subject standing at rest for thirty seconds. After the thirty second resting

recording, the subject performed a fifteen second Valsalva maneuver followed by one minute of recovery recording. All the recorded data was saved in AcqKnowledge in MATLAB data files for processing. The ability of the acquired SCG signal to serve as a proximal reference was then compared to the ICG measurement by evaluating the correlation of changes in PEP measured using the different modalities (R-AO of SCG vs. R-B of ICG). The results of this correlation are detailed in Chapter IV. PPG data recorded using the prototype was not used for this portion of the study.

Next, eight subjects were recruited to further evaluate the performance of the prototype by correlating the changes in SCG based PEP with changes in ICG based PEP after exercise. The same systems were used for this study as the previous study. SCG, PPG, ECG, and ICG data was recorded at rest for one-minute. Next, the subject performed one-minute of intense exercise; no data was recorded during the exercise phase. After the exercise, a five-minute recovery recording was taken as the subject's heightened heart rate returned to the resting state. All the recorded data was saved in AcqKowledge in MATLAB data files for processing. MATLAB was then used to correlate changes in PEP found between SCG and ICG as detailed in the previous study description. The results of this correlation are detailed in Chapter IV.

CHAPTER 4. RESULTS

4.1 Joint Sound Recording System Results

4.1.1 AFE Characterization

The AFE, seen in figure 15, was characterized using the SR785 to test the frequency response (figure 16), total harmonic distortion (figure 17), dynamic range (figure 18), and noise floor (figure 20). The step response (figure 19) was characterized using an Agilent Technologies 33500B True Waveform Generator and Agilent Technologies MSOX-3024A oscilloscope. The characterization results can be seen in the following figures.

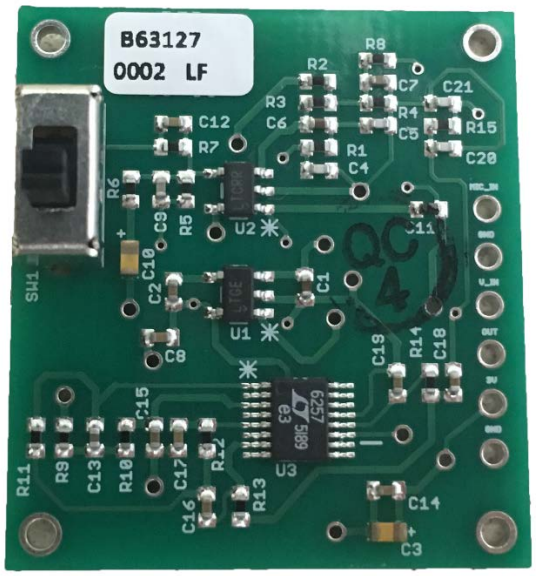

Figure 13: The pre-amplifier AFE designed for joint sound recording with the Knowles BU-23173 contact microphones. The overall PCB dimensions are 1.05”x1.15”.

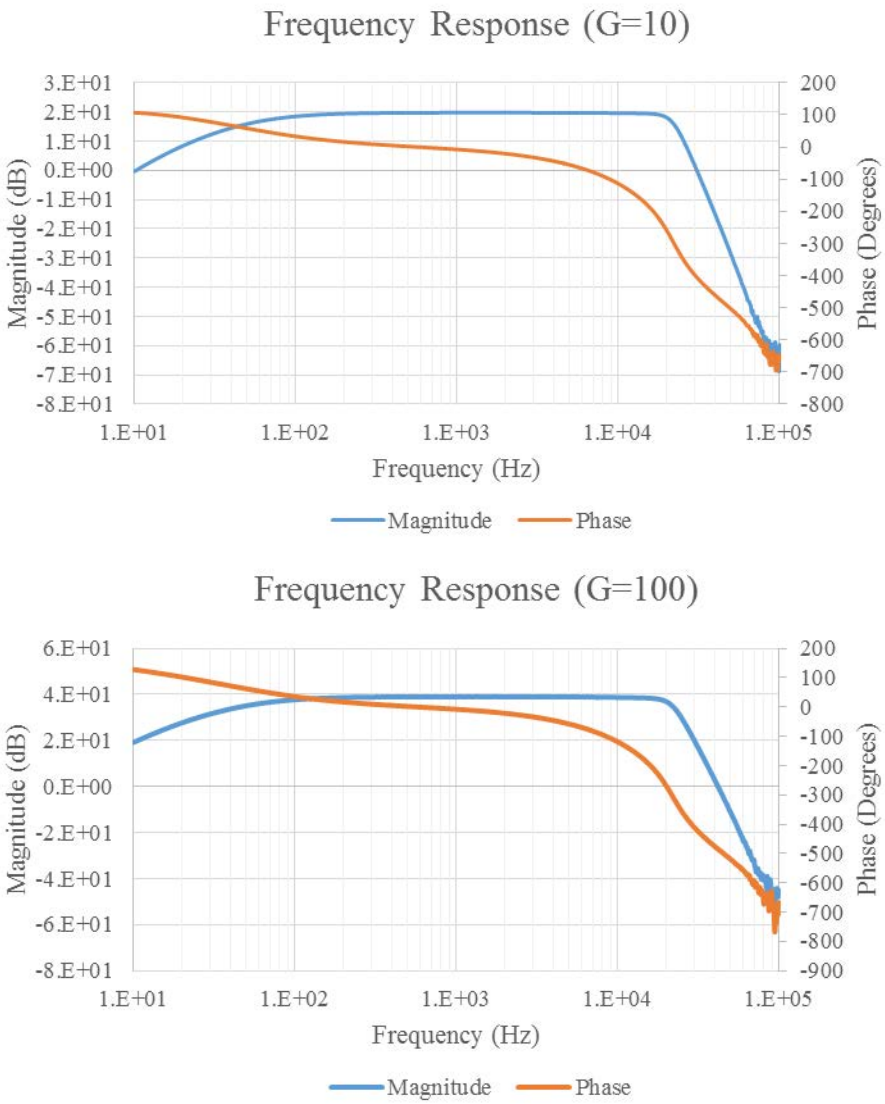

Figure 14: The magnitude (dB) and unwrapped phase (degrees) outputs from the frequency response sweep performed from 10 Hz to 100 kHz with the circuit set to voltage gain of ten (top) and 100 (bottom). The passband gain is 19.7 dB with -3 dB bandpass cutoff frequencies is at 57.6 Hz and 21.4 kHz for the ten voltage gain setting. The passband gain is 39.0 dB with -3 dB bandpass cutoff frequencies is at 59.3 Hz and 20.9 kHz for the 100 voltage gain setting. The test was performed by using the SOURCE channel on the signal analyzer as the input to CH1 on the analyzer and the MIC IN of the AFE with the V OUT of the AFE being connected to CH2 of the analyzer. A swept sine from 10-100 Hz was input to the system with a 10 mV_{RMS} and 1 mV_{RMS} amplitude input to system with the ten voltage gain and 100 voltage gain setting respectively.

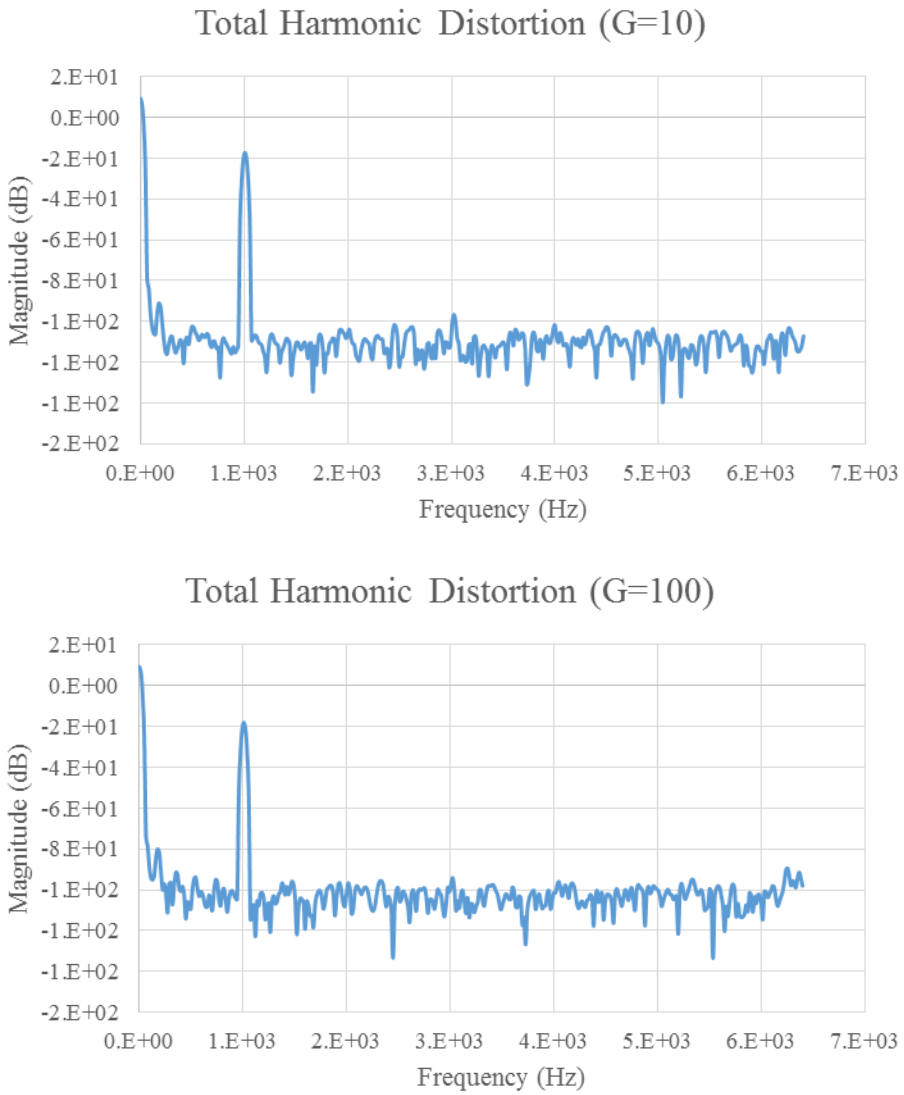

Figure 15: The total harmonic distortion of the circuit was measured by inputting a 10 mV_{RMS} and 1 mV_{RMS} amplitude 1 kHz signal from the SOURCE of the analyzer to the MIC IN of the AFE at the voltage gain ten (top) and 100 (bottom) settings. The THD was measured at the output of the AFE on CH1 to be 0.0122% for the voltage gain ten, and 0.0233% for the gain 100.

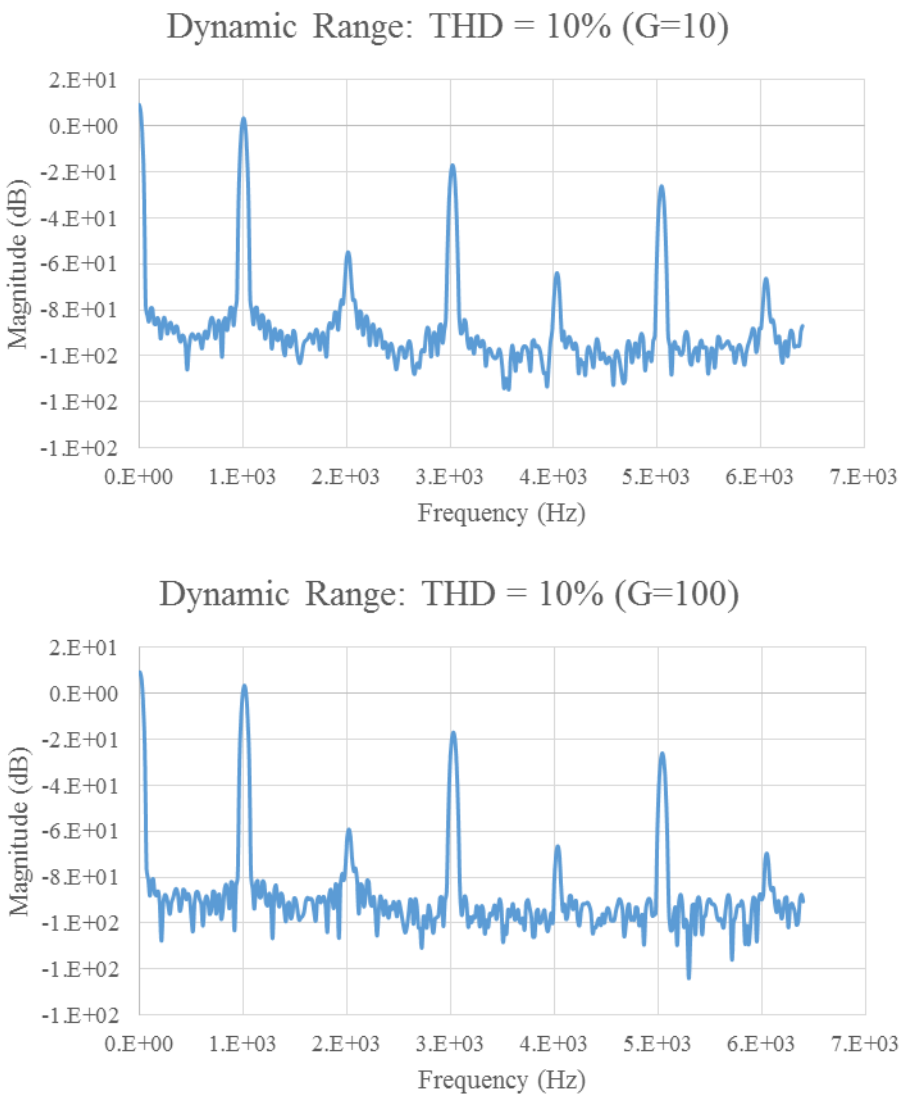

Figure 16: The dynamic range of the AFE was measured by performing the same THD test on the circuit and increasing the RMS voltage of the input 1 kHz signal until the THD output reached 10% of the input value. For the voltage gain ten setting (top) this occurred when the input signal amplitude had been increased to 123.4 mV_{RMS}, and 13.6 mV_{RMS} for the voltage gain 100 setting (bottom).

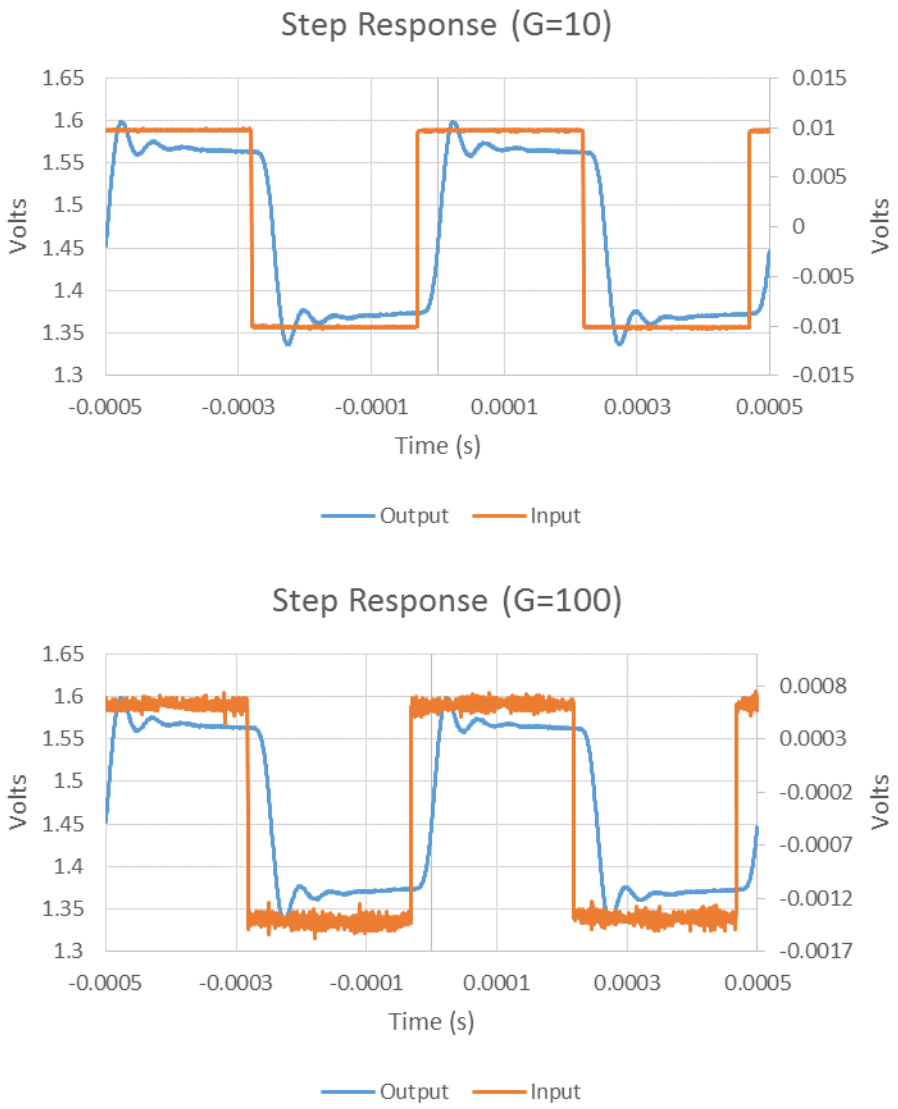

Figure 17: The step response of the AFE was measured by inputting a 2 kHz step function using an Agilent Technologies (Santa Clara, California) 33500B True Waveform Generator with a 20 mV_{P-P} for the voltage gain ten setting (top) and 2 mV_{P-P} for the voltage gain 100 setting input into the MIC IN of the AFE. The output was measured and recorded using an Agilent Technologies MSOX-3024A oscilloscope. For the voltage gain ten setting the rise time of the AFE was 24 µs, the settling time was 118 µs, and the overshoot was 32.0%. For the voltage gain 100 setting the rise time was 23.8 µs, the settling time was 110 µs, and the overshoot was 26.2%.

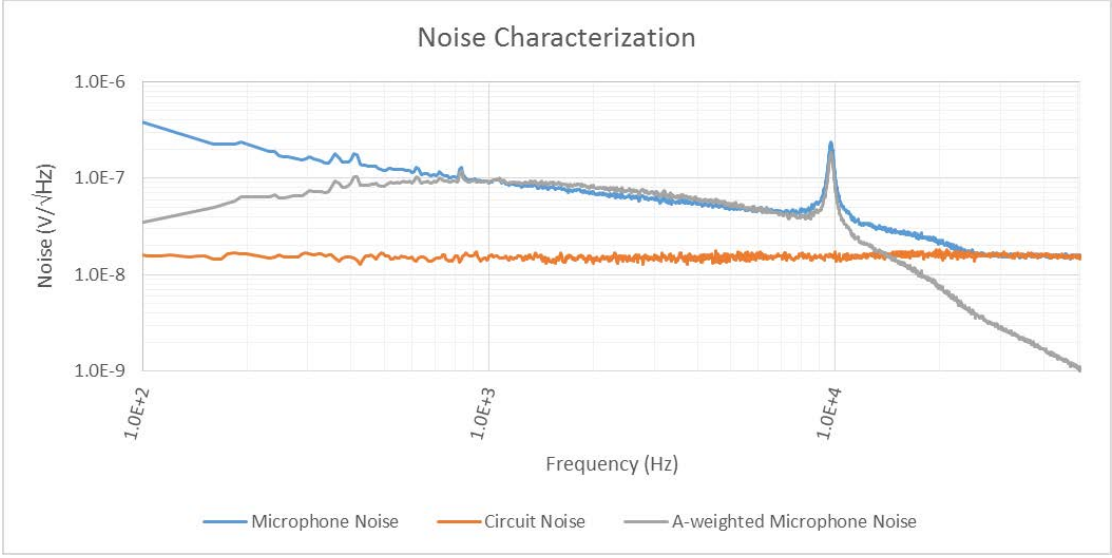

Figure 18: The maximum AFE noise characterization was performed in the voltage gain 100 setting with the microphone connected (microphone and circuit noise) and unconnected (circuit noise only). With the microphone connected and wrapped in Blu Tac (Loctite, Dusseldorf, Germany) to shield the microphone from external noise the output was connected to CH1 of the signal analyser. The noise was largely dominated by the microphone until the 20 kHz cutoff frequency was reached and the system noise became dominated by the white noise of the circuit. A spike in system noise can be seen at 9.87 kHz which is due to the ~10 kHz resonate frequency of the contact microphone specified by the manufacturer. The A-weighted noise calculated with the microphone attached to the circuit is also plotted. The circuit noise was obtained by adding a 5 kΩ resistor to ground to match the microphone output resistance at the XLR connector and connecting the AFE output to CH1 of the signal analyzer. The noise of the circuit is 18 nV/$\sqrt{\mathbf{Hz}}$ throughout the passband, and is negligible when compared to the microphone noise.

4.2 Cuffless Blood Pressure System Results

4.2.1 Quality Classification of PPG Signals

Using the 10-fold cross validation method, the classification algorithm was able to correctly classify 92.8% of the 270 four-second long PPG recordings. Next, another twenty-four minutes of PPG data was recorded from two subjects using the improved array resulting in an additional 360 four-second long PPG segments. This data was used to verify

the classification algorithm by testing its performance on untrained data. The algorithm correctly classified 88.9% of the untrained validation set. The performance of the classification algorithm is further discussed in Chapter V.

4.2.2 SCG Robustness against Position and Pressure Gradient

The method of quantifying the robustness of the LIS344ALH accelerometer as a means of obtaining SCG as a proximal timing reference for PTT is described in section 3.2.3.2. The collected data was then imported into MATLAB where a function was created to extract the time reference of the AO point from the SCG signal for each beat. First, the beats were parsed using the ECG R-peaks. The timing of each R-peak also represented the start of the PEP for every beat. Using the extracted AO feature, the difference in PEP found at positions 1-3, and the effect of the 125-625 gram pressure gradient for three of the four subjects is shown below in table 1 and figure 21. SCG from the omitted subject was extremely compromised by effects of hand tremors and consistent SCG AO peaks could not be obtained. This is further discussed in Chapter V.

Table 1: The average and standard deviation of the PEP found from positions 1-3 based on the applied force gradient of 125, 375, and 625 grams from three subjects. PEP was found using the ECG R-peak and AO feature of the SCG captured using the LIS344ALH accelerometer as detailed in 3.2.3.2.

Subject #	Contact Force	AVG PEP	PEP STD
1	125 g	30.77 ms	1.49 ms
1	375 g	31.77 ms	2.77 ms
1	625 g	28.50 ms	1.87 ms
2	125 g	20.03 ms	2.99 ms
2	375 g	18.53 ms	2.88 ms
2	625 g	18.75 ms	3.08 ms
3	125 g	47.21 ms	1.66 ms
3	375 g	47.47 ms	1.92 ms
3	625 g	46.16 ms	1.84 ms

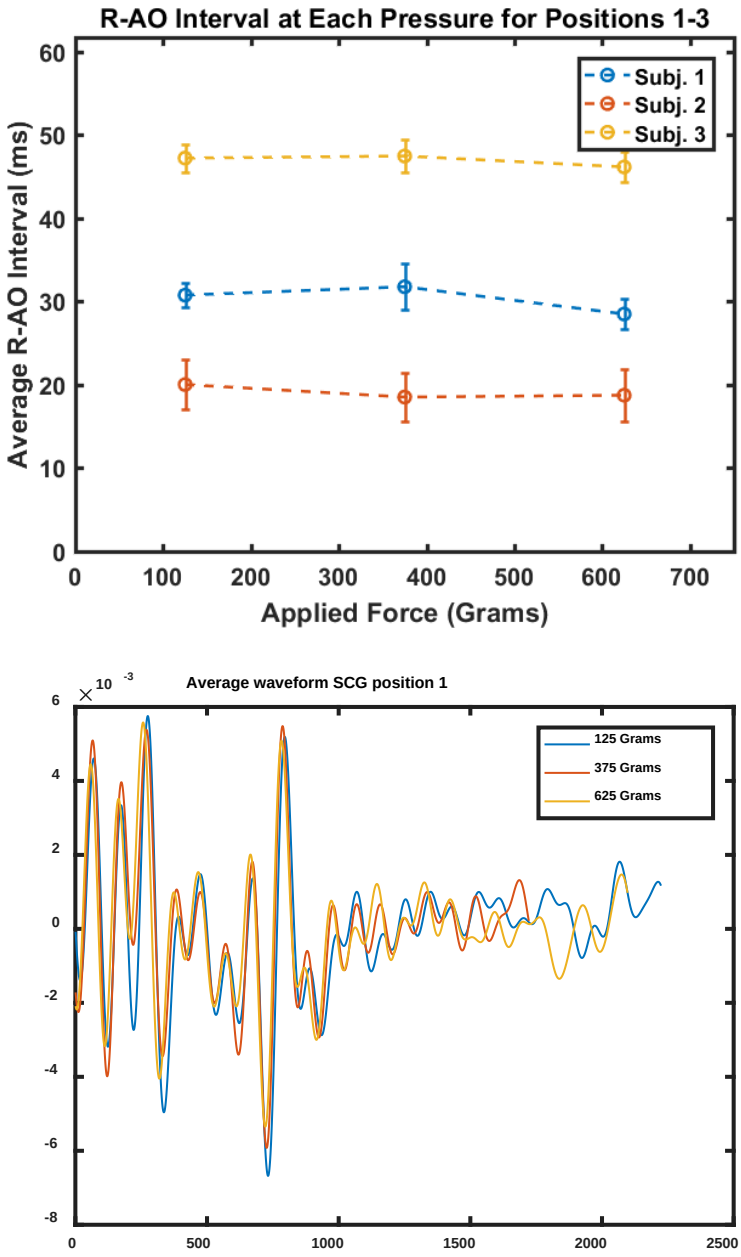

Figure 19: (Top) The plotted effect of contact pressure at positions 1-3 is minimal in the PEP detection using the LIS344ALH as a means of obtaining SCG. The standard deviation of average PEP found between the three pressures is 1.67 ms for subject 1, 0.81 ms for subject 2, and 0.69 ms for subject 3. (Bottom) A plot showing the minute changes in SCG waveform from subject 1 over the pressure gradient.

Using the extracted AO feature, the PEP found at each position was normalized based on position 1 for three of the four subjects. The normalized PEP at each position can be seen in table 2 and figure 22. The results are discussed further in Chapter V.

Table 2: The average PEP found at each position was normalized based on the PEP found at position 1. The normalized data for each subject at each position is included below.

Subject #	Pos 1	Pos 2	Pos 3	Pos 4	Pos 5	Pos 6	Pos 7	Pos 8
1	1	0.87	0.80	0.95	1.27	0.76	2.08	0.92
2	1	0.72	0.80	1.29	1.87	0.81	2.38	1.07
3	1	0.99	0.96	0.88	1.02	0.53	1.39	0.93

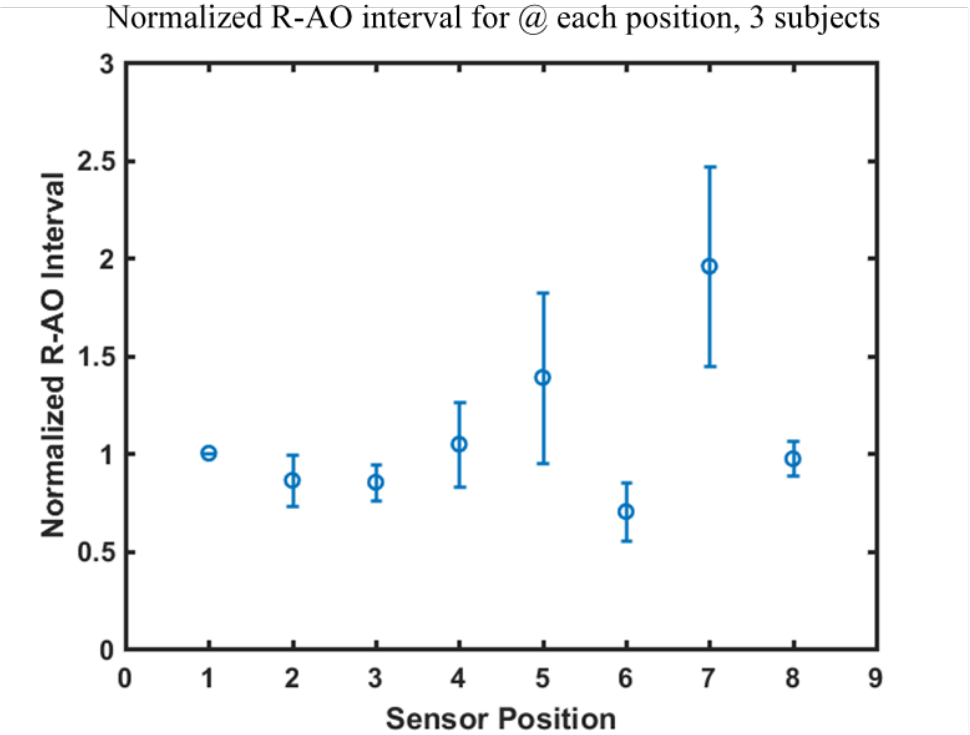

$$n(R-AO)(i) = mean\left(\frac{R-AO_{pos.(i)}}{R-AO_{pos.1}}\right)$$

Figure 20: The average normalized PEP at each position from the three subjects. Positions 1, 2, and 3 are very consistent with one another and the standard deviations at position 2, 3 and 8 are 0.13, 0.09, and 0.088 respectively across the three subjects.

4.2.3 ECG-SCG Correlation with ECG-ICG PEP

As detailed in section 3.2.3.3 the correlation of SCG detected PEP was compared with ICG detected PEP. The results can be seen below in figure 23. The results are further discussed in Chapter V.

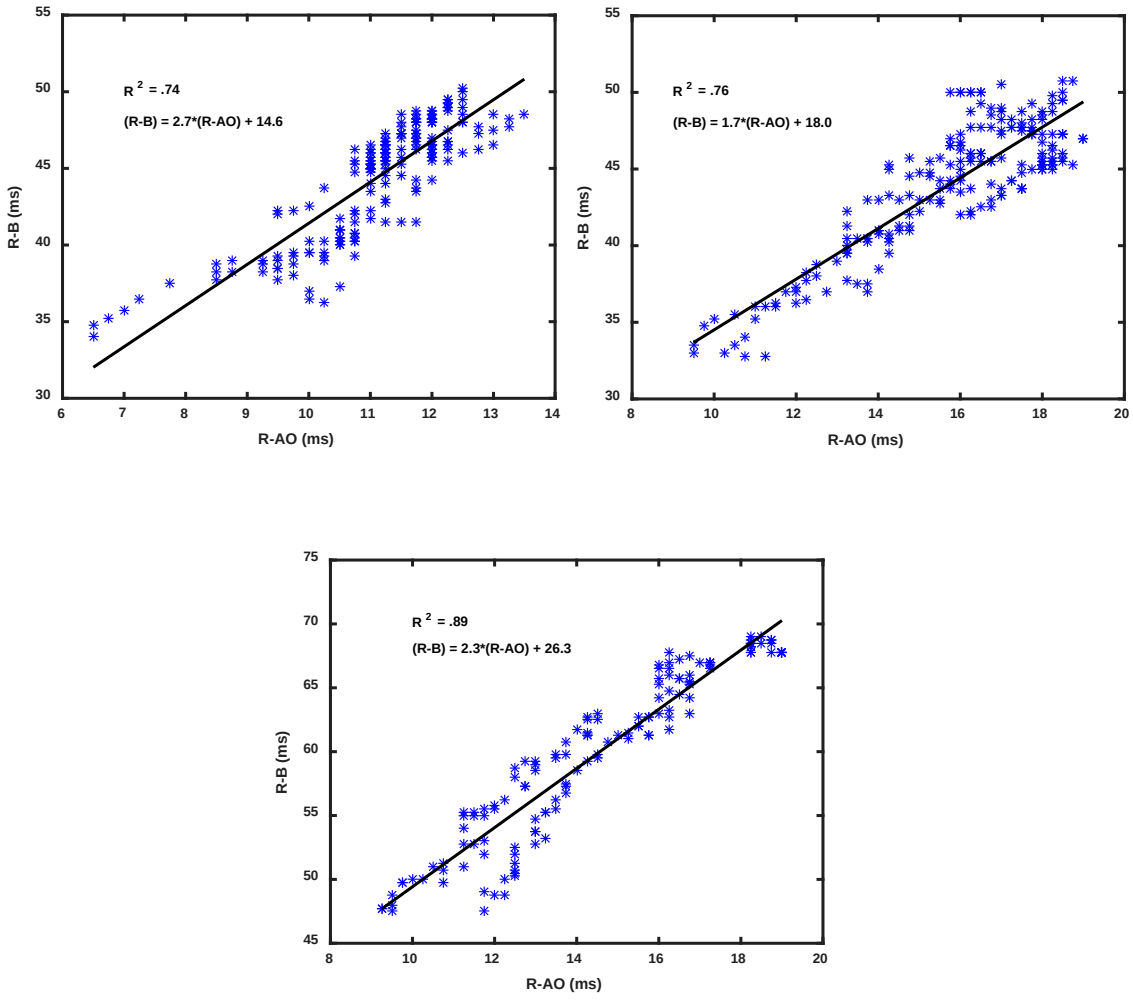

Figure 21: The correlation between changes in SCG detected PEP and ICG detected PEP following Valsalva can be seen for the three subjects used in the study. The R^2 values and relating equation between the R-B interval and R-AO interval are also shown.

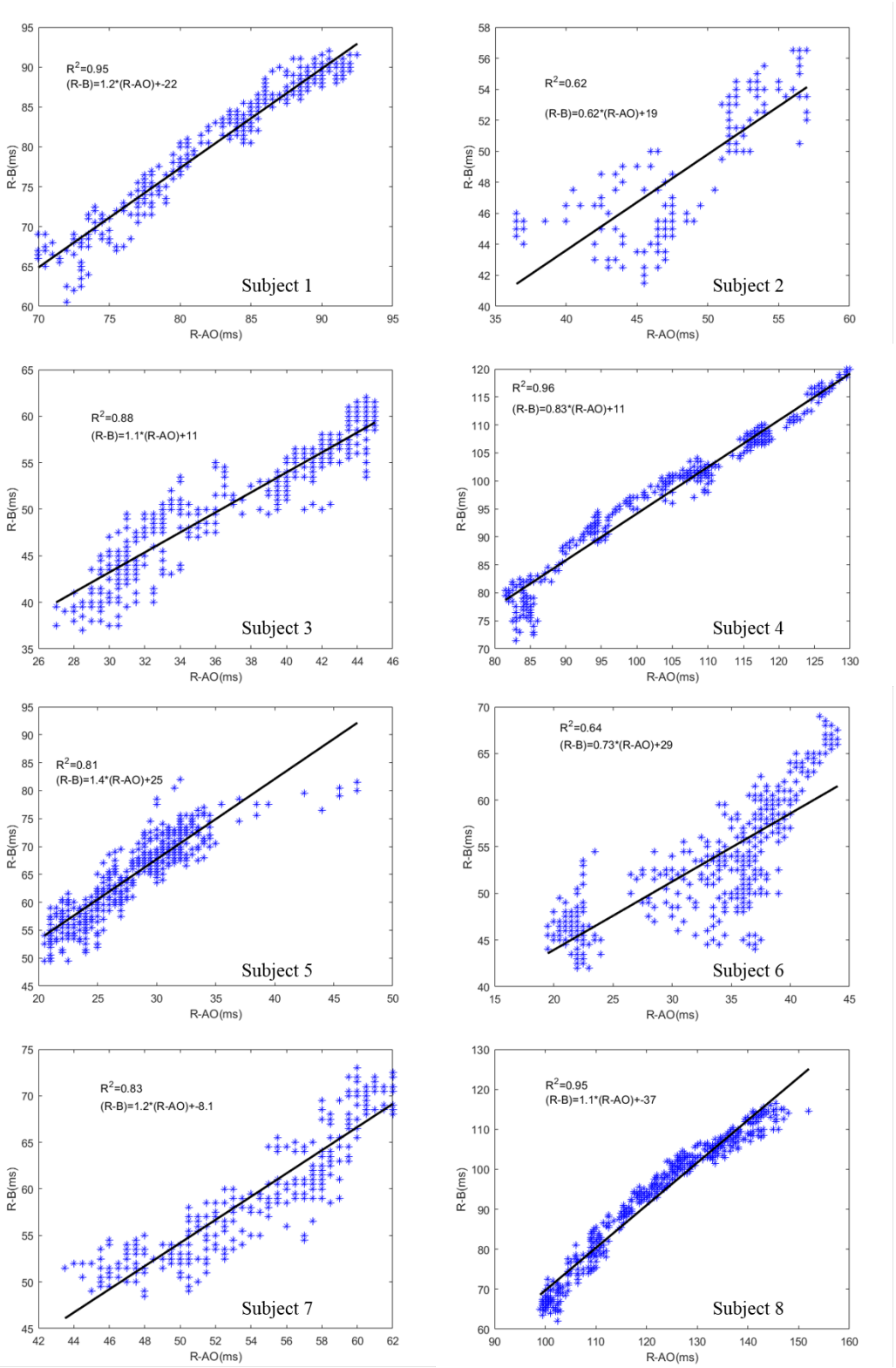

Figure 22: The individual correlations between changes in SCG and ICG detected PEP following exercise can be seen for the eight subjects in the study. The R^2 values and relating equation between the R-B interval and R-AO interval are also shown.

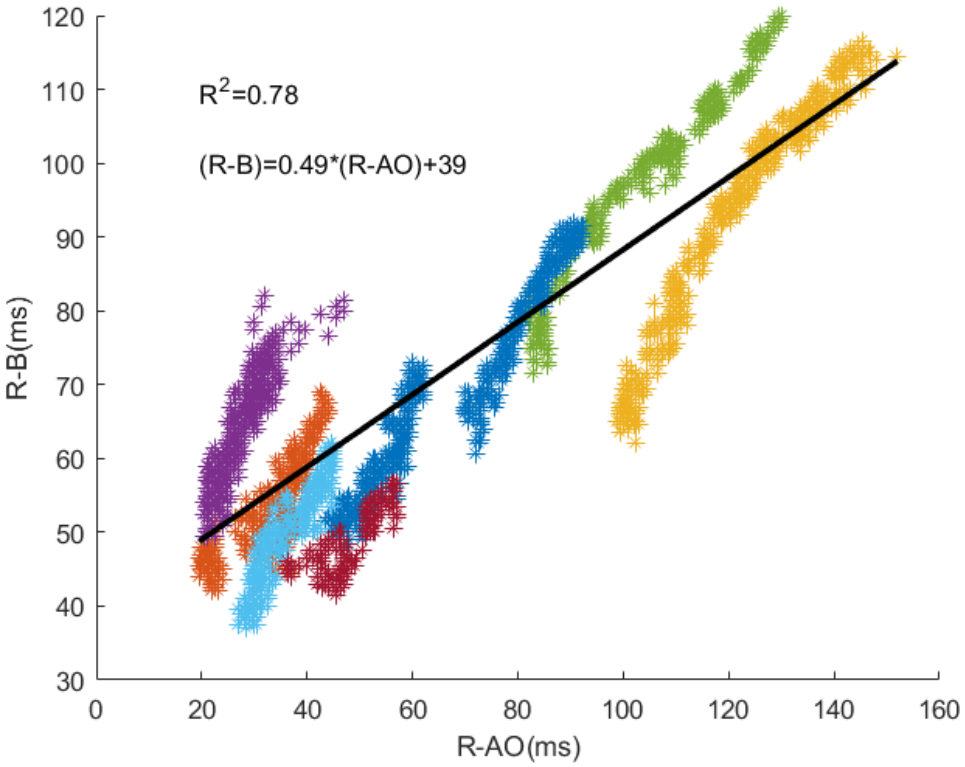

Figure 23: The correlation results for all eight subjects combined between changes in SCG and ICG detected PEP following exercise can be seen. The R^2 value and relating equation between the R-B interval and R-AO interval are also shown.

CHAPTER 5. DISCUSSION

Design considerations for the joint sound recording and cuffless BP measurement systems were focused on capturing clinically relevant data with wearable systems for more frequent out-of-clinic monitoring. Such systems may play a critical role in the development of preventative healthcare, which would greatly reduce cost and improve effectiveness of care compared to the current hospital based system.

The developed joint sound recording system could be used to continuously record knee joint acoustics in- or out-of-clinic at a very low cost. The characterization results of the AFE demonstrated cut-off frequencies within 7% and 4.5% and passband gains within 1.5% and 2.5% of the design specification (for the 20 dB and 40 dB gain settings respectively) with very low harmonic distortion. In addition the AFE makes up only 15.3% of the overall noise of the system with the microphone connected, therefore making the microphone the limiting factor of system noise which is ideal. In addition, by implementing the joint sound system into a compact and lightweight design, joint acoustics during complex movements can now be studied in detail as they relate to quantification of knee joint integrity. Future results from this system could potentially lead to the understanding of acoustical emissions as a meaningful biomarker for osteoarthritis diagnosis and prognosis, as well as develop a better understanding of the effects of the different treatment methods.

The developed cuffless blood pressure systems achieve semi-continuous monitoring of PTT for out-of-clinic BP estimation in both a wearable watch and home based scale design. The real-time classification of PPG signals, coupled with the

implemented array of PPG sensors dramatically improves the robustness of the distal timing detection against user placement error. While the array of PPG sensors triples the coverage area, including low quality signals significantly degrades the overall measurement. Without a classification algorithm, the PPG array could, in fact, reduce the effectiveness of the distal timing reference detection. Since the classification algorithm was able to correctly classify 88.9% of the validation set, it is unlikely that low quality signal from a poorly placed sensor will be included in the distal timing measurement. This ability to utilize an array of sensors, increasing the observed surface area, and classify each output, ensuring low-quality data is disregarded, both increases the reliability of the measured PTT and decreases the amount of time required to obtain a quality distal timing reference for beat-to-beat PTT.

The training set used in the logistic regression included data from multiple individuals with heart rates ranging from 50-100 beats per minute, at several locations over the dorsum of the foot. This is done in an attempt to ensure that the classification is not heart rate or pulse amplitude dependent and can be used for individuals at rest or after exercise. In addition, this also suggests that changes in blood pressure, as a result of arterial stiffening or changes in blood volume, will not cause misclassification of the PPG signal due to changes in pulse volume. Furthermore, since this algorithm is based on simple time and frequency domain features, it could be easily implemented in a common programming language (e.g. Java) for smartphone based PTT extraction systems using PPG as a distal timing reference.

The most significant limitation of the classification algorithm is the five-second recording time required to produce a FFT frequency resolution of 0.2 Hz when sampling

at 2 kHz. This does not allow for immediate classification and could result in a significant amount of recording time to obtain a quality distal waveform if the array is misplaced several times in succession. This could be mitigated in the future by increasing the number of PPG sensors included in the array resulting in even greater coverage area.

For the wearable prototype, the use of the LIS344ALH accelerometer proved to be robust against placement error so long as the measurement was taken with the accelerometer held against the lower half of the sternum. Placement over the thoracic cage and upper sternum were not able to produce consistent results for use as a proximal timing reference for PTT. In addition, the negligible changes in mean and variance in R-AO measured across the tested force gradient prove that the system is very robust against changes in contact pressure. However, it was clear that the presence of hand movements in an individual can severely degrade the quality of the SCG measurement. Future design of the watch based system must account for such tremors and become more robust against their effects.

The strong individual correlations of changes in PEP found using the SCG based watch versus traditional ICG ($R^2 > 0.81$ for subjects 1, 3-5, 7-8) demonstrate that the proposed concept is a suitable method for obtaining a proximal timing reference for PTT measurement. Furthermore, an R^2 value of 0.78 for the aggregated subject data shows a strong correlation of detected PEP between the eight subjects. However, extraction of the AO feature proved to be difficult between subjects due to variance in the individual SCG waveform shapes. This complicates the AO extraction and requires the use of ICG to determine the AO feature from each subject's SCG waveform. As a result, unless a more universal AO extraction method can be developed, any individual intending to use this

watch based BP estimation system would need to be individually assessed in-clinic to determine the specific AO feature based on an ICG calibration.

Poor correlation results from subjects 2 and 6 are a result of a poorly defined AO feature present in the SCG waveforms for these individuals. This resulted in the implemented AO detection algorithm occasionally selecting incorrect features as the AO point. Further investigation into a more robust and universal AO extraction method on a larger subject sample size is needed to determine the most optimal means of PEP extraction using the watch based SCG system. In addition, a lower noise accelerometer may be required to ensure the AO peak is more prominent in comparison to the sensor noise.

CHAPTER 6. CONCLUSION

Chronic diseases affect a large percentage of the aging population and will continue to place stress on global healthcare systems as this segment of the population continues to grow (i.e. people are living longer). Osteoarthritis and hypertension are two of the most common chronic diseases which affect older adults, and can significantly diminish an individual's quality of life. More personalized and preventative care for these diseases is dependent upon the ability to identify early risk factors and continuously monitor the effects of treatment. Currently there are no known biomarkers, apart from imaging techniques such as X-ray and MRI, which can aid in the diagnosis or prognosis of osteoarthritis, and out-of-clinic hypertension monitoring can only be performed by bulky oscillometric devices.

The AFE designed for the joint sound recording system offers a small, ultra-low noise, and wide-band design to improve the measured signal quality for characterization of the knee joint acoustics as they correlate to specific injuries which will be performed in future studies with this system. In addition, the system was implemented in a wearable design to allow for untethered recording during complex movements. The improved PPG array, and quality classification algorithm implemented in the scale based system are pertinent to any future BP estimation system using PPG as a distal timing reference for PTT measurement. The watch SCG based system further improves this design to be wearable, allowing for more continuous BP tracking where the home-based scale cannot be conveniently used. The future work on this system will require the correlation of changes in measured BP with PTT for subjects with and without hypertension. In addition,

the variability in the SCG waveform between subjects should be explored to extract the features which are common between all subjects.

The systems presented in this document were designed to be used for more continuous out-of-clinic monitoring of knee joint acoustics and blood pressure estimation by capturing longitudinal biomechanical measurements indicative of the chronic disease state of an individual dealing with OA or hypertension. However, because of the nature of the measured biomechanical signals, the systems must be designed to be robust against user error to eliminate the continuous need of a medical professional. This results in increased emphasis on the physical system design to ensure robust sensor interfaces, the analog circuitry to reduce measurement noise, and signal processing to provide automated classification and feedback improve out-of-clinic measurement quality. The progress detailed in this document outlines significant steps toward the realization of non-invasive assessment of biomechanical signals to improve the efficiency and effectiveness of health care providers serving the aging population.

REFERENCESBIBio

[1] T. M. Dall, P. D. Gallo, R. Chakrabarti, T. West, A. P. Semilla, and M. V. Storm, "An aging population and growing disease burden will require a large and specialized health care workforce by 2025," *Health affairs (Project Hope)*, vol. 32, p. 2013, 2013.

[2] W. W. Hung, J. S. Ross, K. S. Boockvar, and A. L. Siu, "Recent trends in chronic disease, impairment and disability among older adults in the United States," *BMC Geriatrics*, vol. 11, pp. 47-47, 2011.

[3] S. World Health Organization, *Preventing chronic diseases : a vital investment*: Place of publication not identified World Health Organization, 2005.

[4] "Prevalence and most common causes of disability among adults--United States, 2005," *MMWR. Morbidity and mortality weekly report*, vol. 58, p. 421, 2009.

[5] C. C. Y. Ya-Li Zheng, B. P. L. Xiao-Rong Ding, B. P. L. Poon, B. P. L. Lo, B. P. L. Heye Zhang, B. P. L. Xiao-Lin Zhou, *et al.*, "Unobtrusive Sensing and Wearable Devices for Health Informatics," *Biomedical Engineering, IEEE Transactions on*, vol. 61, pp. 1538-1554, 2014.

[6] V. K. Varadan, *Mobile wearable nano-bio health monitoring systems with smartphones as base stations*. New York, N.Y. : New York, N.Y. (222 East 46th Street, New York, NY 10017): New York, N.Y. : Asme

New York, N.Y. 222 East 46th Street, New York, NY 10017 : Momentum Press, 2012.

[7] C. f. D. C. a. Prevention. (2016, August 5). *Athritis-Related Statistics*. Available: http://www.cdc.gov/arthritis/data_statistics/arthritis-related-stats.htm

[8] J. W. Bijlsma, F. Berenbaum, and F. P. Lafeber, "Osteoarthritis: an update with relevance for clinical practice," *The Lancet*, vol. 377, pp. 2115-2126, 2011.

[9] J. T. Sharp, J. Angwin, M. Boers, J. Duryea, G. von Ingersleben, J. R. Hall, *et al.*, "Computer based methods for measurement of joint space width: update of an ongoing OMERACT project," *J Rheumatol*, vol. 34, pp. 874-83, Apr 2007.

[10] K. Kim, J. Seo, and C. Song, "An Acoustical Evaluation of Knee Sound for Non-invasive Screening and Early Detection of Articular Pathology," *Journal of Medical Systems*, vol. 36, pp. 715-722, 2012.

[11] H. Oka, S. Muraki, T. Akune, A. Mabuchi, T. Suzuki, H. Yoshida, *et al.*, "Fully automatic quantification of knee osteoarthritis severity on plain radiographs," *Osteoarthritis and Cartilage,* vol. 16, pp. 1300-1306, 2008.

[12] T. Conrozier, A. M. Tron, P. Mathieu, and E. Vignon, "Quantitative assessment of radiographic normal and osteoarthritic hip joint space," *Osteoarthritis and cartilage,* vol. 3 Suppl A, p. 81, 1995.

[13] T. L. Boegård, O. Rudling, I. F. Petersson, and K. Jonsson, "Joint space width of the tibiofemoral and of the patellofemoral joint in chronic knee pain with or without radiographic osteoarthritis: a 2-year follow-up," *Osteoarthritis and Cartilage,* vol. 11, pp. 370-376, 2003.

[14] F. W. Roemer, F. Eckstein, D. Hayashi, and A. Guermazi, "The role of imaging in osteoarthritis," *Best Practice & Research Clinical Rheumatology,* vol. 28, pp. 31-60, 2014.

[15] H. Toreyin, S. Hersek, C. N. Teague, and O. T. Inan, "A Proof-of-Concept System to Analyze Joint Sounds in Real Time for Knee Health Assessment in Uncontrolled Settings," *Sensors Journal, IEEE,* vol. 16, pp. 2892-2893, 2016.

[16] C. N. Teague, S. Hersek, H. Toreyin, M. L. Millard-Stafford, M. L. Jones, G. F. Kogler, *et al.*, "Novel Methods for Sensing Acoustical Emissions From the Knee for Wearable Joint Health Assessment," *Biomedical Engineering, IEEE Transactions on,* vol. 63, pp. 1581-1590, 2016.

[17] C. Institute of Medicine . Committee on a National Surveillance System for and D. Select Chronic, *A nationwide framework for surveillance of cardiovascular and chronic lung diseases*. Washington, D.C.: Washington, D.C. : National Academies Press, 2011.

[18] L. Landsberg, L. J. Aronne, L. J. Beilin, V. Burke, L. I. Igel, D. Lloyd-jones, *et al.*, "Obesity-related hypertension: Pathogenesis, cardiovascular risk, and treatment—A position paper of the The Obesity Society and the American Society of Hypertension," *Obesity,* vol. 21, pp. 8-24, 2013.

[19] P. Gianfranco, E. O. Juan, L. Carolina, and B. Grzegorz, "Assessment and management of blood-pressure variability," *Nature Reviews Cardiology,* vol. 10, p. 143, 2013.

[20] J. Mallett, *Critical Care Manual of Clinical Procedures and Competencies*. Hoboken: Hoboken : Wiley, 2013.

[21] J. Sola, M. Proenca, D. Ferrario, J.-A. Porchet, A. Falhi, O. Grossenbacher, *et al.*, "Noninvasive and Nonocclusive Blood Pressure Estimation Via a Chest Sensor," *Biomedical Engineering, IEEE Transactions on,* vol. 60, pp. 3505-3513, 2013.

[22] M. A. Younessi Heravi, M. A. Khalilzadeh, and S. Joharinia, "Continuous and Cuffless Blood Pressure Monitoring Based on ECG and SpO2 Signals ByUsing Microsoft Visual C Sharp," *Journal of biomedical physics & engineering,* vol. 4, p. 27, 2014.

[23] W. Chen, T. Kobayashi, S. Ichikawa, Y. Takeuchi, and T. Togawa, "Continuous estimation of systolic blood pressure using the pulse arrival time and intermittent calibration," *Medical and Biological Engineering and Computing,* vol. 38, pp. 569-574, 2000.

[24] D. B. Bak and L. Lading, "Quantitative determination of arterial pulse wave velocity by non-interfering bioimpedance sensing," ed, 2011, pp. 6442-6445.

[25] N. Luo, W. Dai, C. Li, Z. Zhou, L. Lu, C. Poon, *et al.*, "Flexible Piezoresistive Sensor Patch Enabling Ultralow Power Cuffless Blood Pressure Measurement," *Advanced Functional Materials,* vol. 26, pp. 1178-1187, 2016.

[26] C.-S. Kim, A. M. Carek, R. Mukkamala, O. T. Inan, and J.-O. Hahn, "Ballistocardiogram as Proximal Timing Reference for Pulse Transit Time Measurement: Potential for Cuffless Blood Pressure Monitoring," *Biomedical Engineering, IEEE Transactions on,* vol. 62, pp. 2657-2664, 2015.

[27] A. Verma, R. Fazel-Rezai, J. Zanetti, and K. Tavakolian, "Preliminary Results for Estimating Pulse Transit Time Using Seismocardiogram," *Journal Of Medical Devices-Transactions Of The Asme,* vol. 9, 2015.

[28] G. Zhang, M. Gao, D. Xu, N. B. Olivier, and R. Mukkamala, "Pulse arrival time is not an adequate surrogate for pulse transit time as a marker of blood pressure," *Journal of applied physiology (Bethesda, Md. : 1985),* vol. 111, p. 1681, 2011.

[29] L. A. Geddes, M. H. Voelz, C. F. Babbs, J. D. Bourland, and W. A. Tacker, "Pulse Transit Time as an Indicator of Arterial Blood Pressure," *Psychophysiology,* vol. 18, pp. 71-74, 1981.

[30] R. Mukkamala, J.-O. Hahn, O. T. Inan, L. K. Mestha, C.-S. Kim, H. Toreyin, *et al.*, "Toward Ubiquitous Blood Pressure Monitoring via Pulse Transit Time: Theory and Practice," *Biomedical Engineering, IEEE Transactions on,* vol. 62, pp. 1879-1901, 2015.

[31] S. L. O. Martin, A. M. Carek, C. Kim, H. Ashouri, O. T. Inan, J. Hahn, R. Mukkamala, "Weighing Scale Based Pulse Transit Time is a Superior Marker of Blood Pressure than Conventional Pulse Arrival Time," *Scientific Reports, In Press*.

[32] C. B. Frank, R. M. Rangayyan, and G. D. Bell, "Analysis of knee joint sound signals for non-invasive diagnosis of cartilage pathology," *Engineering in Medicine and Biology Magazine, IEEE,* vol. 9, pp. 65-68, 1990.

[33] K. S. Kim, J. H. Seo, J. U. Kang, and C. G. Song, "An enhanced algorithm for knee joint sound classification using feature extraction based on time-frequency analysis," *Computer Methods and Programs in Biomedicine,* vol. 94, pp. 198-206, 2009.

[34] E. Stojakovic. (2014). *Weight Bearing Knee X-Ray*. Available: https://www.flickr.com/photos/akasped/15462121754

[35] G. McHugh. (2015). *Knee Arthroplasty*. Available: http://www.gavinmchughorthopaedics.com/knee-arthroplasty.html

[36] N. Dilmen. (2012). *Knee MRI*. Available: https://commons.wikimedia.org/wiki/File:Knee_MRI_113532.png

[37] S. C. Abbott and M. D. Cole, "Vibration arthrometry: a critical review," *Critical reviews in biomedical engineering,* vol. 41, p. 223, 2013.

[38] H. Toreyin, H. K. Jeong, S. Hersek, C. N. Teague, and O. T. Inan, "Quantifying the Consistency of Wearable Knee Acoustical Emission Measurements During Complex Motions," *IEEE journal of biomedical and health informatics,* vol. 20, p. 1265, 2016.

[39] C. Wheatley, E. Snyder, M. Joyner, B. Johnson, and T. Olson, "Comparison of intra-arterial and manual auscultation of blood pressure during submaximal exercise in humans," *Applied Physiology, Nutrition, and Metabolism,* vol. 38, p. 537, 2013.

[40] (2016). *Blood Pressure*. Available: https://commons.wikimedia.org/wiki/File:100_Blood_Pressure.jpg

[41] A. Gadini. *Blood Pressure Care*. Available: https://pixabay.com/en/unit-of-pressure-meter-990462/

[42] B. S. Alpert, D. Quinn, and D. Gallick, "Oscillometric blood pressure: a review for clinicians," *Journal of the American Society of Hypertension,* vol. 8, pp. 930-938, 2014.

[43] H. Skirton, W. Chamberlain, C. Lawson, H. Ryan, and E. Young, "A systematic review of variability and reliability of manual and automated blood pressure readings," in *J. Clin. Nurs.* vol. 20, ed, 2011, pp. 602-614.

[44] W. Wojciechowska, K. Stolarz-Skrzypek, K. Kawecka-Jaszcz, J. A. Staessen, J.-G. Wang, H. European Project on Genes in, *et al.*, "Cross-sectional and longitudinal assessment of arterial stiffening with age in European and chinese populations," *Frontiers in Physiology,* 2012.

[45] A. Sherwood, M. T. Allen, J. Fahrenberg, R. M. Kelsey, W. R. Lovallo, and L. J. P. Doornen, "Methodological Guidelines for Impedance Cardiography," *Psychophysiology,* vol. 27, pp. 1-23, 1990.

[46] B. J. M. Van Der Meer, J. P. P. M. D. Vries, W. O. Schreuder, E. R. Bulder, L. Eysman, and P. M. J. M. D. Vries, "Impedance cardiography in cardiac surgery patients: abnormal body weight gives unreliable cardiac output measurements," *Acta Anaesthesiologica Scandinavica*, vol. 41, pp. 708-712, 1997.

[47] O. T. Inan, P.-F. Migeotte, K.-S. Park, M. Etemadi, K. Tavakolian, R. Casanella, *et al.*, "Ballistocardiography and Seismocardiography: A Review of Recent Advances," *Biomedical and Health Informatics, IEEE Journal of,* vol. 19, pp. 1414-1427, 2015.

[48] *Medical instrumentation : application and design*, 3rd ed.. ed. New York: New York : Wiley, 1998.

[49] D. M. Salerno and J. Zanetti, "Seismocardiography for Monitoring Changes in Left Ventricular Function during Ischemia," *Chest,* vol. 100, pp. 991-993, 1991.

[50] Y. Maeda, M. Sekine, and T. Tamura, "Relationship Between Measurement Site and Motion Artifacts in Wearable Reflected Photoplethysmography," *Journal of Medical Systems,* vol. 35, pp. 969-976, 2011.

[51] O. T. Inan, L. Dookun Park, G. T. A. Giovangrandi, and G. T. A. Kovacs, "Noninvasive Measurement of Physiological Signals on a Modified Home Bathroom Scale," *Biomedical Engineering, IEEE Transactions on,* vol. 59, pp. 2137-2143, 2012.

[52] M. A. Hall and G. Holmes, "Benchmarking attribute selection techniques for discrete class data mining," *Knowledge and Data Engineering, IEEE Transactions on,* vol. 15, pp. 1437-1447, 2003.